



Switching extensional and contractional tectonics in the West Kunlun Mountains during the Jurassic period: responses to the Neo-Tethyan geodynamics along the Eurasian margin

Hong-Xiang Wu^{1,2}, Han-Lin Chen^{1,2}, Andrew V. Zuza³, Yildirim Dilek⁴, Du-Wei Qiu^{1,2}, Qi-Ye Lu^{1,2}, Feng-Qi Zhang^{1,2}, Xiao-Gan Cheng^{1,2}, and Xiu-Bin Lin^{1,2}

¹School of Earth Sciences, Zhejiang University, Hangzhou, China

²Research Center for Structure in Oil and Gas Bearing Basins, Ministry of Education, Hangzhou, China

³Nevada Bureau of Mines and Geology, Nevada Geosciences, University of Nevada, Reno, NV, USA

⁴Department of Geology and Environmental Earth Science, Miami University, Oxford, OH, USA

Correspondence: Han-Lin Chen (hlchen@zju.edu.cn)

Received: 3 June 2024 – Discussion started: 10 June 2024

Revised: 14 December 2024 – Accepted: 31 December 2024 – Published: 21 February 2025

Abstract. The Tethyan orogenic belt records a long-lived geological cycle involving subduction and collision along the southern margin of the Eurasian continent. The West Kunlun Mountains, located at the junction between the Tibetan and Pamir orogens within the Tethyan realm, records multiple orogenic events from the Paleozoic to the Cenozoic that shape the northwestern Tibetan Plateau. However, deciphering the complex Mesozoic contractional and extensional tectonics to interpret the broader Tethyan geodynamics remains challenging. To address the tectonic transition following the early Cimmerian (Late Triassic) collision, this study investigates the newly identified Jurassic sedimentary strata and volcanic rocks in the West Kunlun Mountains. Zircon geochronological results of basalts and sandstones reveal that this ~ 2.5 km thick package was deposited at ca. 178 Ma, rather than in the previously reported Neoproterozoic age. The alkaline basalts at the top of the formation exhibit chemical compositions similar to oceanic island basalts, consistent with the intracontinental extension environment revealed by the upward-fining sedimentary pattern. Provenance analysis, including conglomerate clast lithologies and detrital zircons, suggests a substantial contribution from adjacent basement sources, likely influenced by the normal faulting during initial rift stage. These findings indicate that the West Kunlun Mountains rapidly transitioned into an extensional setting after suturing with Cimmerian terranes. The regional structure, stratigraphy, and magmatism suggest that the Early–

Middle Jurassic southwestern Tarim Basin was subsequently inverted during the Late Jurassic and earliest Cretaceous. We propose that the Mesozoic deformational history in the West Kunlun Mountains was related to the northward subduction of the Neo-Tethys Ocean, as it transitioned from southward retreat to northward flat-slab advancement. Comparing with the entire strike length of the Eurasian Tethyan orogen, we find that the subduction mode varied from the west to the east, reflecting the broad geodynamic changes to, or initial conditions of, the Neo-Tethyan system.

1 Introduction

The Tethyan orogenic belt is an over 15 000 km trans-Eurasian orogenic system with a series of mountain chains and orogenic plateaus (Fig. 1a; Şengör, 1987; Metcalfe, 2013; Wu et al., 2020). The evolution of the Tethyan orogenic belt involved multiple phases of ocean basin opening and closure (i.e., the Proto-, Paleo-, and Neo-Tethys oceans) throughout the Phanerozoic era, which resulted in the development of multiple orogenic belts across the Eurasian continent (Stampfli, 2000; Wan et al., 2019; Metcalfe, 2021). The complex history of accretionary and collisional orogenesis in the Tethyan realm is intricately linked to the breakup and formation of two mega-landmasses, namely Gondwana and Laurasia (Şengör et al., 1988; Stampfli and Borel, 2002; Zuza

and Yin, 2017; Li et al., 2018; Wang et al., 2018). Documenting the mode and nature of the accretionary and collisional events in the Mesozoic history of the Tethyan orogenic system is, therefore, important for understanding the continental dynamics of Eurasia.

The Mesozoic Tethyan orogenic belt involved orogenesis, rifting, and basin evolution, which are associated with the convergence between the southern Asian margin and Cimmerian terranes derived from Gondwana (e.g., Kazmin, 1991; Stampfli and Borel, 2002; Angiolini et al., 2013; Robinson, 2015). The Mesozoic tectonic evolution of the Tethyan realm exhibits significant variations from the west to the east (Şengör, 1984; Zhu et al., 2022). In the west Asian section of the Tethyan orogenic belt, geochronological and geochemical data from different magmatic rock assemblages suggest a northwestward-propagating continental rift system along the southern margin of the central Iran Block during the Early Jurassic to Early Cretaceous (Hunziker et al., 2015; Lechmann et al., 2018; Azizi and Stern, 2019). This process is envisioned to have been associated with subduction geodynamics involving multiple intraoceanic subduction zones, slab tearing, and alternating slab rollback and advance within the Neo-Tethys (Zhang et al., 2018; Jafari et al., 2023). Conversely, in the east Asian section of the Tethyan orogenic belt (i.e., Tibetan sector), an Andean-type orogeny along the southern margin of Eurasia from the Early Jurassic to the Early Cretaceous has been proposed to explain deformation and sedimentation patterns in the southern Tibetan Plateau (Kapp et al., 2007; Zhang et al., 2012; Xie and Dilek, 2023). This process was punctuated by Toarcian–Aalenian back-arc rifting event resulting from retreat of the subducting Neo-Tethyan seafloor (Hou et al., 2015; Wei et al., 2017).

The West Kunlun Mountains, stretching from the northern Pamir to northwestern Tibetan Plateau, occupy a critical position at the junction between the western and eastern Tethyan orogenic belts (Fig. 1b; Şengör, 1984; Wu et al., 2016). The West Kunlun Mountains involved the closure of the Paleo-Tethys Ocean in the Triassic–Jurassic, followed by Cenozoic deformation and uplift during the Himalayan orogeny (Mattern and Schneider, 2000; Cao et al., 2015; Li et al., 2019; Xiao et al., 2002). Hence, the Mesozoic geology of the West Kunlun Mountains documents the plate tectonic history of the junction region within the Tethyan realm, providing pivotal insights into the formation of this extensive orogenic system. In particular, the Cimmerian Orogeny in the West Kunlun region critically records the collision between the Gondwana-derived continental fragments and the southern Eurasian margin in the latest Triassic to late Jurassic (e.g., Şengör, 1979), but the timing and duration of this orogen remains equivocal. Existing interpretations of the Jurassic paleogeography and evolution vary, ranging from synorogenic (Cao et al., 2015) and post-orogenic (Wu et al., 2021) to transtensional (Sobel, 1999), because of the scarcity of the relevant geological record from this period. Significant challenges also persist in understanding the Mesozoic evo-

lution of the Pamir terranes (Angiolini et al., 2013), including the timing of suturing and exact kinematics of related deformation (Robinson, 2015). The Cenozoic contractional deformation episodes, due to the northward subduction of the Neo-Tethyan Ocean and the collision of India with Eurasia, further complicate our understanding in this remote region (Burtman and Molnar, 1993; Cowgill, 2010). The limited knowledge of the Jurassic and Cretaceous evolution of the Pamir interior has been preliminarily deduced from the timing and nature of regional magmatic activities (Chapman et al., 2018) that are challenged by the information derived from the surrounding fragmented sedimentary basins (Leith, 1985; Wu et al., 2021).

To better understand the regional evolution and tectonomagmatic processes in the West Kunlun Mountains, we have undertaken a systematic geochronological and geochemical study and detailed analyses of the sedimentary provenance of volcanoclastic rock suites in the Jurassic Kyzyltau–Kandilik basin. By integrating these new results with existing data from the adjacent region, this study provides further constraints on the Mesozoic tectonic history of the central junction of the Tethyan orogenic belt and probes the preceding processes that cause the formation of the broad plateau in central Asia.

2 Geological framework and sampling

2.1 Tethyan history

The Tethyan orogenic belt separates the main Eurasian cratons and stable platforms in the north from Gondwana-derived continental terranes in the south (e.g., Şengör et al., 1988; Stampfli et al., 1991). The development of the Tethyan orogenic belt involves the evolution of multiple ocean basins and their seaways, including the Proto-Tethys, Paleo-Tethys, and Neo-Tethys (Stampfli, 2000; Metcalfe, 2021). These ancient ocean basins overlapped in time but closed successively as the Gondwana-derived ribbon continents (i.e., Apulia, Pelagonia, Sakarya, Tauride, South and North Qiangtang, and Lhasa) accreted to the southern margin of Eurasia, creating several sub-parallel suture zones stretching from the circum-Mediterranean region, Caucasus, Iranian plateau, and continuing eastward into the Tibetan Plateau and Southeast Asia (Fig. 1a; Dilek and Moores, 1990; Wu et al., 2020; Metcalfe, 2021).

The Cenozoic indentation of the Pamirs fundamentally affected the deformation pattern of the Tethyan orogenic belt and geographically divided the belt into western and eastern sectors (Tapponnier et al., 1981). The history of the Proto-Tethys was linked to the breakup of the Rodinia supercontinent (Zhao et al., 2018). The western segment of the Proto-Tethys has been defined as a Cambrian–Silurian ocean existing between Baltica and Gondwana, whereas the eastern Proto-Tethys appears to have been closed earlier in the Early

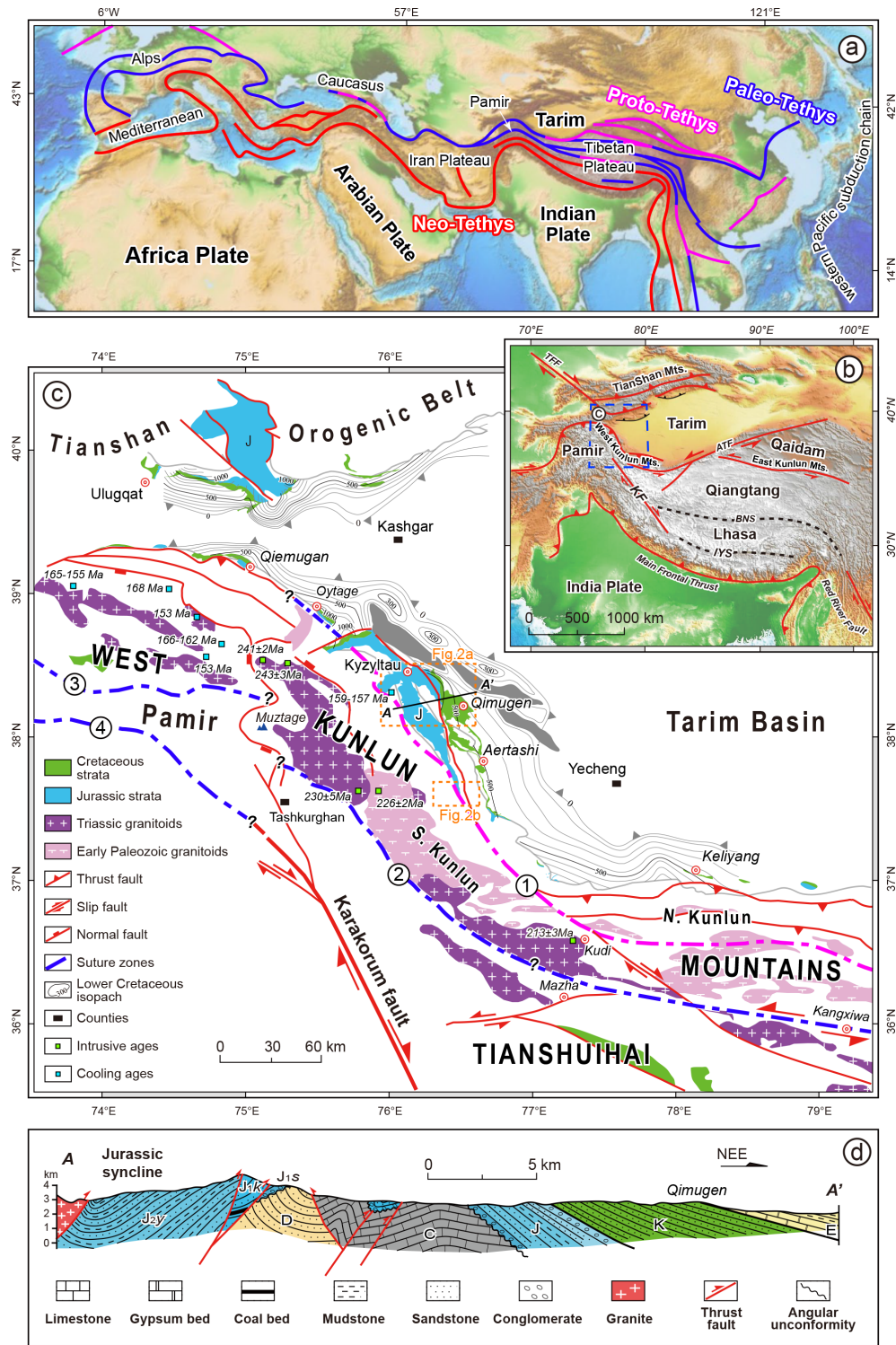


Figure 1. (a) Tectonic plate framework in the Northern Hemisphere and the suture zones within the Tethyan realm (modified from Wu et al., 2020). (b) Structural framework of central Asia showing main blocks and orogenic belts, with locations of major sutures and boundary faults. TFF is for Talas–Fergana Fault, BNS is for Bangong–Nujiang suture, IYS is for Indus–Yarlung suture, and ATF is for Altyn–Tagh fault. (c) Simplified geologic map of the West Kunlun Mountains, including major units and suture zones (modified from Wu et al., 2021; cooling ages of basements refer to Yang et al., 2017), namely the ① Early Paleozoic Kudi suture, ② Triassic Mazar–Kangxiwa suture, ③ Triassic Tanymas suture separating the north and central Pamirs, and ④ Rushan–Pshart suture zone separating the central and south Pamirs. (d) A section across the eastern part of the West Kunlun Mountains showing the deformed and fragmented Jurassic basin. The section location is presented in Fig. 1c.

Silurian as a series of Asian blocks collided onto the northern margin of Gondwana (e.g., Stampfli and Borel, 2002). The opening of the Paleo- and Neo-Tethyan ocean basins was related to slab pull forces that caused the detachment of the Hun (including the Tarim and North and South China) and Cimmerian terrane ribbons from the northern margin of Gondwanaland, respectively (Stampfli and Borel, 2002; Ruban et al., 2007). These terranes were successively transferred northward to the Eurasian continent, causing the closure of these internal seaways during the Cimmerian and Himalayan orogenies at the end of the Triassic and the beginning of the Cenozoic, respectively (Dilek and Furnes, 2019; Wan et al., 2019).

The final demise of the Paleo-Tethyan Ocean and the initiation of subduction in the Neo-Tethyan Ocean occurred simultaneously in the Triassic–earliest Jurassic, which is of vital importance for comprehension of the cyclical Tethyan evolution (Wan et al., 2019). The West Kunlun Mountains, situated to the north of the Pamir syntaxis, form the western extent of the Tibetan Plateau (Fig. 1b and c). They constitute an important spatial link between the western and eastern domains of the Tethyan orogenic belt. The formation of the West and East Kunlun Mountains involved accretionary and collisional orogenesis during the closure of the Proto-Tethys and Paleo-Tethys oceans (Mattern and Schneider, 2000; Xiao et al., 2005; Dong et al., 2018). The East Kunlun Mountains are displaced to the north relative to the West Kunlun Mountains by the dextral Altyn-Tagh strike-slip fault (Fig. 1b). During the Early Paleozoic, the closure of the Proto-Tethys Ocean led to the collision of the Tarim Craton (northern Kunlun) and the southern Kunlun terrane along the Kudi suture zone (Fig. 1c; Zhang et al., 2019a). After splitting from eastern Gondwana in the Devonian–Carboniferous, the Tianshuihai–Qiangtang blocks traveled northward towards the Tarim Craton because of the subduction of the Paleo-Tethyan Ocean. These blocks ultimately collided with the Tarim Craton at the latest Triassic, forming the Mazar–Kangxiwa suture zone (Fig. 1c; Xiao et al., 2005; Metcalfe, 2021). The Pamir terranes (including the central Pamir, south Pamir, and Karakoram), commonly regarded as the western counterpart of the Qiangtang block, rifted from Gondwana during the Permian (Robinson, 2015; Angiolini et al., 2015). The major Cimmerian orogenic unconformity between the Lower Jurassic and the deformed Upper Triassic strata is generally considered to mark the timing of the amalgamation of these Pamir terranes onto the Eurasian margin (Angiolini et al., 2013; Li et al., 2022).

The mid-Mesozoic tectonic evolution of the West Kunlun Mountains and Pamir is somewhat enigmatic, as the first-order geodynamic mechanisms for widespread deformation remain unclear. Several major exhumation events, including the Late Triassic and Early Jurassic, Middle–Late Jurassic, Early Cretaceous, and Late Cretaceous, are documented by low-temperature thermochronology in the mountain ranges and surrounding basins (Sobel et al., 2013; Cao

et al., 2015; Li et al., 2019, 2023). Mid-Cretaceous granitoids are widespread in the south Pamir and Karakoram. A Jurassic to Cretaceous polymetamorphic history is also displayed by monazite ages (Faisal et al., 2014). The basement cooling, as well as magmatic activities, and metamorphic events have previously been interpreted as associated with far-field stress effects of collisional events (Yang et al., 2017) or retro-arc contraction during an Andean-type subduction of the Neo-Tethyan Ocean (Chapman et al., 2018). These Mesozoic structures within the orogenic belts were intensely reworked by the Cenozoic deformation during the Himalayan orogeny (Burtman and Molnar, 1993).

2.2 Regional geology and sampling strategy

This study focused on the central and southern parts of the northwest-trending Jurassic basin within the West Kunlun Mountains (Fig. 1c). The Kyzyltau region, situated in the central part of this Jurassic basin, preserves thick Early–Middle Jurassic strata. It mainly comprises the Lower Jurassic Shalitashi and Kangsu formations and the Middle Jurassic Yangye and Taerga formations (Fig. 2a). The Shalitashi Formation comprises a massive, thick conglomerate that overlies the deformed Carboniferous and Permian shallow-marine clastic rocks and limestones along an angular unconformity (Fig. 3a). The poorly sorted textures and lateral thickness variations in the conglomerate indicate that its clastic material originated from alluvial fans (Sobel, 1999; Fig. 3b–e). The Kangsu and Yangye formations form the main part of the Jurassic strata (Fig. 2a), with total stratigraphic thickness exceeding 1800 m. The Kangsu Formation mainly comprises stacked greywackes interbedded with coal layers. The Yangye Formation consists mainly of interbedded sandstones and shales exhibiting typical Bouma sequences, indicative of turbidite deposits in a deepwater environment (Wu et al., 2021). The Middle Jurassic Taerga Formation is only exposed in the northeastern side of the region and consists of thinly bedded shales and siltstones. The Lower to Middle Jurassic stratigraphy forms an upward-fining sequence, indicating the expanding and deepening of the basin over time. Structurally, the Jurassic strata exhibit a strong deformation, forming a northwest-trending synclinorium (Fig. 2a). The Cenozoic contraction in the region extensively deformed the coal-bearing strata, resulting in the formation of multi-scale folds and thrusts (Fig. 3f and g). Regionally, the Early–Middle Jurassic strata are unconformably overlain by the Late Jurassic Kuzigongsu Formation and the Cretaceous Kezilesu Group, which are characterized by massive oxidation-colored conglomerate and sandstones (Fig. 3h). Synchronous unconformities also exist in the south Qiangtang and Bangong–Nujiang suture zones (Ma et al., 2017a, 2018).

In the Kandilik region, geological mapping identified a coal-bearing formation, known as the Lower–Middle Jurassic Yarkant Formation, and a massive conglomerate classi-

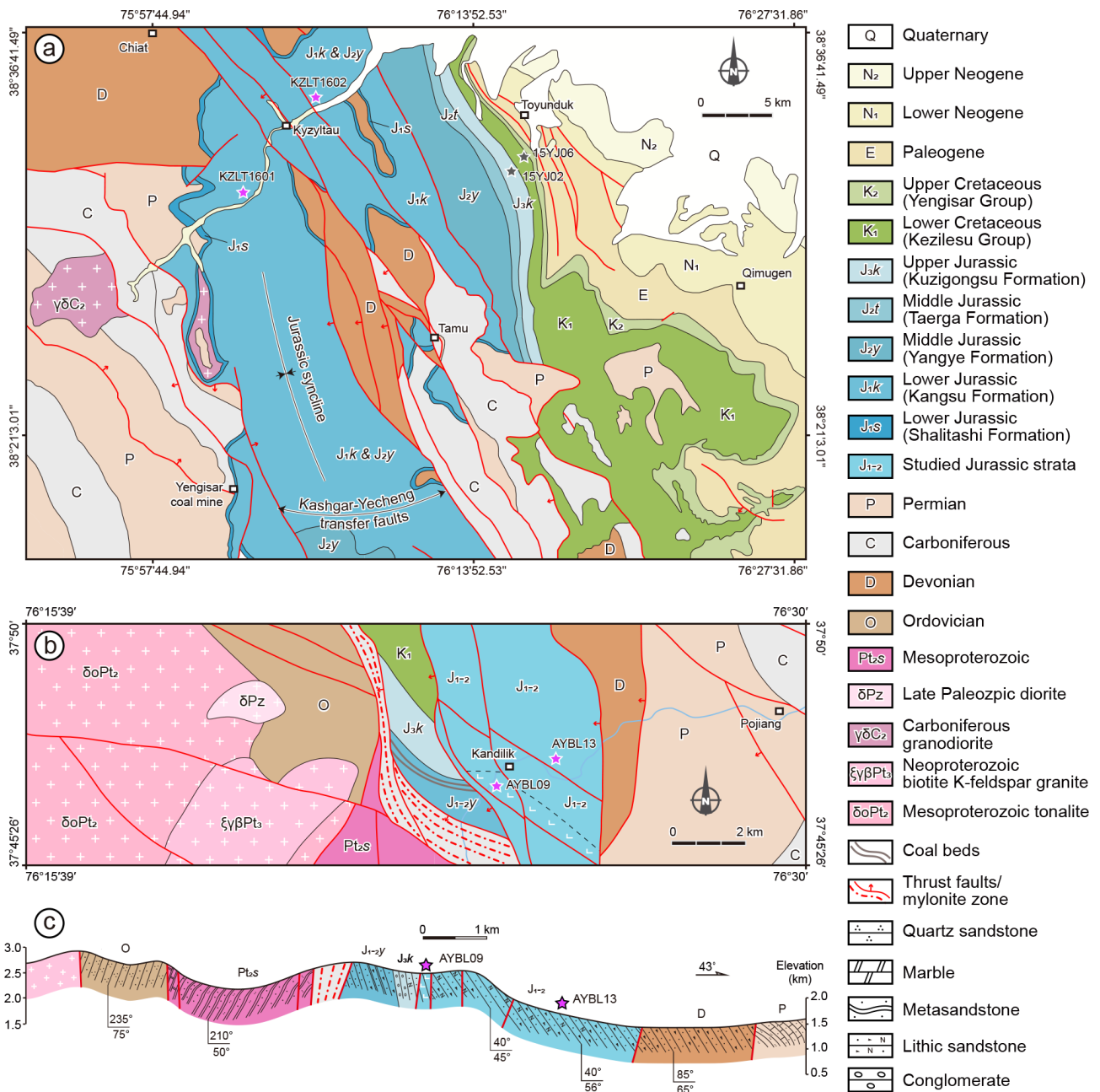


Figure 2. (a) Geological map in the Kyzyltau region showing the stratigraphic information and sampling locations. (b) Geological map in the Kandilik region showing the Proterozoic basements and Paleozoic–Mesozoic strata. The red stars mark sampling locations in this work, and the grey stars mark the locations of published data (Zhang et al., 2019b). (c) A field geological section showing the regional strata and deformation along the Pojiang river in Fig. 2b.

fied as the Upper Jurassic Kuzigongsu Formation (Fig. 2b). These Jurassic strata were strongly deformed and laterally bounded by a mylonitic shear zone to the west and thrust faults to the east. A stratigraphic unit consisting of gray–black mudstone, siltstone, and fine sandstone is exposed to the east of the Yarkant Formation, with a thickness exceeding 3500 m (Ma et al., 1991). Abundant mafic dikes intruded into the lower part of the strata (Fig. 3i), causing local contact

metamorphism. A suite of volcanic strata composed of several basalt layers are juxtaposed with the thick clastic package along a steeply dipping fault. Several eruptive episodes are identified within this unit based on alternating volcanic horizons, including volcanic breccia (Fig. 3j), amygdaloidal basalts, and massive basalts (Fig. 3k). These volcanic rocks belong to the part of upper member deposited above the thick clastic strata (Ma et al., 1991). Due to the lack of reliable con-

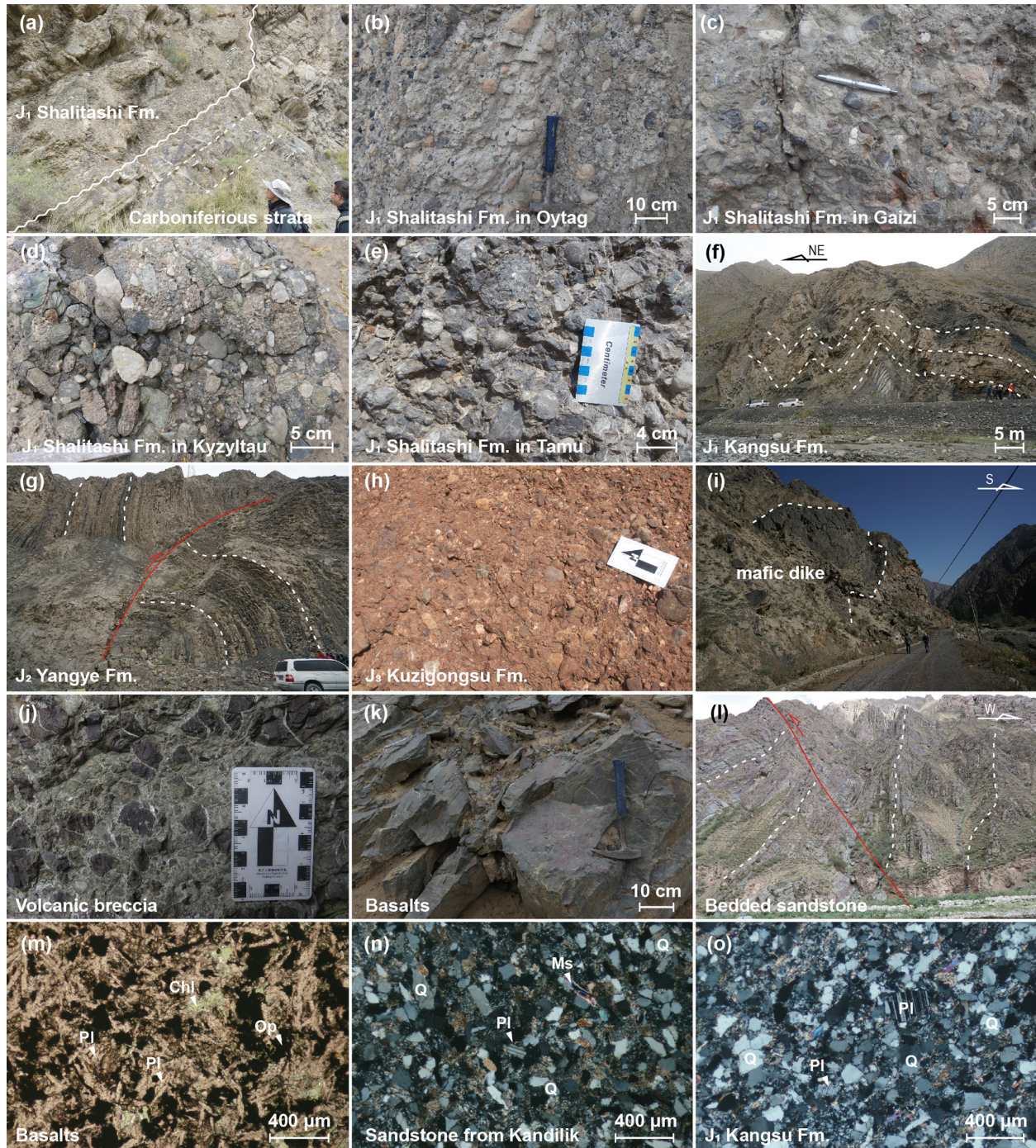


Figure 3. Photographs showing the observation from the field and a binocular microscope. (a) Early Jurassic Shalitashi Formation overlying on the deformed Carboniferous strata with angular unconformity. (b) Conglomerate clast lithologies of the Shalitashi Formation in Oyttag, (c) Gaizi, (d) Kyzyltau, and (e) Tamu. (f) Early Jurassic Kangsu Formation with strongly deformed sandstone layers. (g) Strong deformation of the turbidite sequences in the Middle Jurassic Yangye Formation. (h) Conglomerate clast lithologies in the Late Jurassic Kuzigongsu Formation. (i) Mafic dike within newly identified Jurassic strata in the Kandilik region. (j) Basaltic volcanic breccia. (k) Massive basalt layer. (l) Jurassic bedded feldspar lithic sandstones with great thickness, which was previously assigned to be Precambrian age. (m) Micrograph of basalt under plane-polarized light. (n) Micrograph of Jurassic sandstone under cross-polarized light from Kandilik section. (o) Micrograph of Jurassic sandstone under cross-polarized light from Kyzyltau section. Pl is for plagioclase; Chl is for chlorite; Op is for opaque mineral (mainly Ti–Fe oxides); Q is for quartz.

straints from chronological results, this stratigraphic unit has long been thought of as Precambrian in age (Ma et al., 1991). Structurally, the strata were intensely deformed by regional Kashgar–Yecheng transfer faults (Fig. 2), and the bedding dips steeply to the northeast (Fig. 3l).

In the Kandilik region, one basalt sample (AYBL09) was collected near the thrust fault for geochronological dating (Fig. 2b). Six fresh and undeformed basalt samples were also obtained away from faults for geochemical analysis. These basaltic rock samples consist primarily of plagioclase with a fine columnar texture and anhedral Ti–Fe oxides (Fig. 3m). Plagioclase is locally altered into chlorite. Additionally, one quartz–lithic sandstone sample (AYBL13) was collected for detrital zircon age analysis. This sample exhibits poor sorting and is composed mainly of quartz (~ 30 %) with angular shapes, feldspar (< 10 %), and lithic fragments (> 60 %) (Fig. 3n). For regional comparison, two sandstone samples were collected from the Kangsu (KZLT1601) and Yangye formations (KZLT1602) in the Kyzyltau region (Fig. 2a). These sandstones show similar textures and compositions to the clastic sample from the Kandilik region (Fig. 3o).

3 Methodology

One basalt sample (AYBL09) was collected from the Kandilik section (Fig. 2b) for zircon U–Pb geochronology and in situ trace-element analysis. Zircon separation and cathodoluminescence (CL) imaging were done at Yu-Heng Rock and Mineral Technology Service Co., Ltd., Langfang, China. Zircons were analyzed for U–Pb geochronology using an Agilent 8900 triple quadrupole inductively coupled plasma mass spectrometry (ICP-QQQ) equipped with an ESI New Wave NWR193UC (Two Vol2) laser ablation system at Beijing Quick-Thermo Science and Technology Co., Ltd, China. Concordia plots were constructed using IsoplotR (Vermeesch, 2018).

To analyze the petrogenesis and tectonic setting of magmatism, six fresh basalt rocks were collected from the same section to determine their major and trace-element chemistry. Samples were first crushed and then powdered in an agate mill. Elemental analyses were conducted at Wuhan SampleSolution Analytical Technology Co., Ltd. Major element analyses were performed by X-ray fluorescence spectrometry (ZSX Primus II), with analytical uncertainties generally better than 1 %. Trace-element contents were determined using an Agilent 7700e ICP-MS.

To compare the detrital age patterns and sedimentary provenance, we have conducted zircon U–Pb dating on two sandstones (KZLT1601 and KZLT1602) exposed in the Kyzyltau section and on one sandstone (AYBL13) exposed in the Kandilik section (Fig. 2b). Zircons from samples KZLT1601 and KZLT1602 were analyzed for U–Pb geochronology using a Thermo Fisher iCAP RQ ICP-MS equipped with a Teledyne CETAC Analyte HE laser abla-

tion system at the School of Earth Sciences, Zhejiang University. Zircons from sample AYBL13 were analyzed for U–Pb geochronology using an Agilent 8900 ICP-QQQ equipped with an ESI New Wave NWR193UC (Two Vol2) laser ablation system at Beijing Quick-Thermo Science and Technology Co., Ltd. The common Pb was corrected with the method proposed by Andersen (2002). Concordia plots and kernel density estimate (KDE) plots were constructed using IsoplotR (Vermeesch, 2018) and DensityPlotter 8.5 (Vermeesch, 2012), respectively.

The details of the analytical procedures and the information of the analytical methodologies, as explained above, are presented in Sect. S1 in the Supplement.

The data from the conglomerate in the Shalitashi Formation were collected at eight different sections. Analysis of conglomerate clasts was conducted within a designated 1 m² area. Our focus was on documenting the lithological compositions of the clasts, with at least 100 gravel types randomly counted at each site.

4 Analytical results

4.1 Morphology and geochronology of zircons from basalt sample

The results of zircon U–Pb dating of the basalt sample are presented in Table S1 in the Supplement. Approximately 170 zircon grains have been successfully separated from the basalt sample. Zircon crystals are mostly transparent and colorless, displaying varying lengths ranging between 50–200 μm with elongation ratios of 1 : 1–5 : 1 (Fig. 4). Upon an examination of their cathodoluminescence (CL) images, we have sub-categorized these zircons into two groups based on the presence of oscillatory zoning. The grains showing well-defined growth zoning (type 1) are generally sub-euhedral in shape (no. 3 in Fig. 4), implying their magmatic origin (Fig. 4; Hoskin and Schaltegger, 2003). Another type (type 2) of zircon displays an inconspicuous zoning texture (no. 4 in Fig. 4) or yields only faintly visible zoning patterns (no. 15 in Fig. 4). A morphological analysis of these zircons reveals a range from needle-shaped and elongated crystals (no. 13 in Fig. 4) to stubby and equant forms (no. 12 in Fig. 4). A common feature of these varying grains is their subrounded external appearance. This may result from moderate resorption either during the evolution of the magma chamber when the magma is oversaturated with respect to zircon or a certain degree of metamorphism (Corfu et al., 2003). In addition to their “polished” shape, these zircons commonly display nebulous or patchy-zoned centers without distinct core–rim structures (no. 11–13 in Fig. 4).

We have conducted a total of 36 spot analyses on various types of zircons (Fig. 4), resulting in 33 analyses with a > 90 % concordance (Fig. 5a). The Th/U ratios of all tested zircons range from 0.04 to 1.52 (Fig. 5d). We cannot assert that

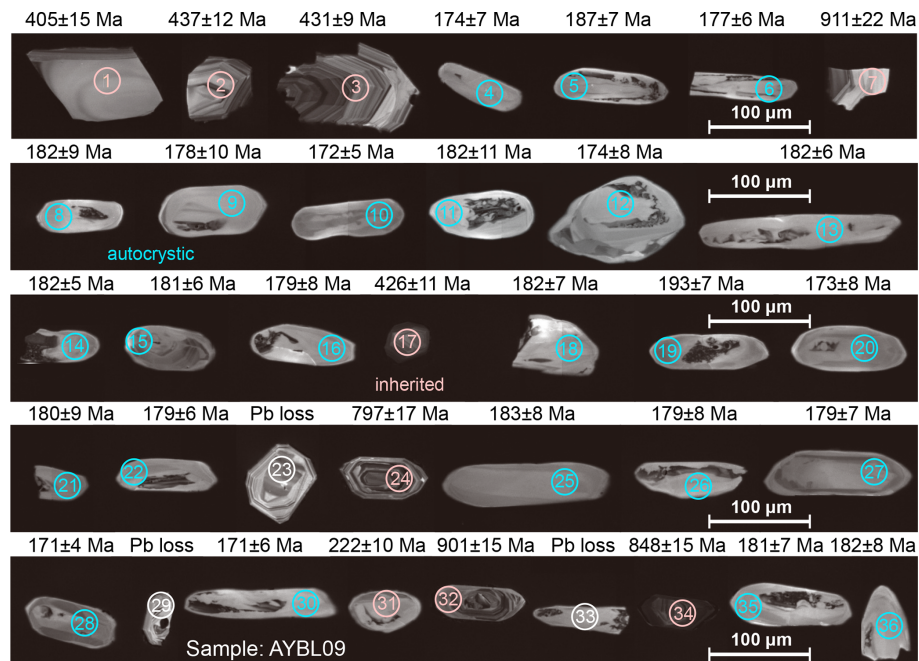


Figure 4. CL images of all tested zircon varieties in basalt sample AYBL09, noting the apparent $^{206}\text{Pb}/^{238}\text{U}$ ages above. The red circle indicates the target points of type 1 zircon, the blue circle represents the target points of type 2 zircon, and the white circle marks the points where discordant ages were obtained.

all of them are primary crystals without modification simply based on the evaluation of Th/U ratios. However, all of these results yielded concordant ages spanning a broad range from the Early Neoproterozoic to the Jurassic. Type 1 zircon grains have Th/U ratios ranging from 0.38 to 1.44, while type 2 zircon grains exhibit a wider range. Based on the classification and statistical analysis of zircon characteristics, we found that type 1 zircons, which commonly exhibit clear oscillatory zoning, have older $^{206}\text{Pb}/^{238}\text{U}$ ages ranging from 405 to 911 Ma, whereas type 2 zircons display uniform ages between 168 and 193 Ma (Table S1). The 20 youngest zircons with concordant ages define a weighted mean $^{206}\text{Pb}/^{238}\text{U}$ age of 178 ± 2 Ma (MSWD = 0.99) (Fig. 5b). We interpret this Toarcian age as the crystallization age of this rock sample. The remaining older zircons yield primarily middle-Paleozoic and Neoproterozoic ages, which we interpret as being inherited from the country rock.

4.2 Whole-rock major and trace elements of basalts

The chemical compositions of the basalt samples from the Kandilik section are provided in Table S3 in the Supplement. Except for one sample (AYBL11D), the majority of our samples display similar geochemical compositions characterized by low SiO_2 (45.7–51.0 wt %) and MgO (4.78–7.18 wt %) contents and Mg#s ranging between 45 and 52. These samples possess high TiO_2 (2.42–3.34 wt %) and total alkali ($\text{Na}_2\text{O} + \text{K}_2\text{O} = 5.17$ –6.35 wt %) contents and exhibit moderate Al_2O_3 contents ranging from 11.1 to 14.4 wt % and

total Fe_2O_3 ranging from 12.6 to 13.7 wt %. In comparison, the sample AYBL11D displays relatively high contents of SiO_2 (55.5 wt %) and TiO_2 (4.76 wt %), with a low total alkali content (4.80 wt %). All basalt samples fall within the alkaline series field as depicted in the total alkali–silica diagram (Fig. 6a). However, it is worth noting that all analyzed samples exhibit varying loss-on-ignition (LOI = 1.51–9.81 wt %) values attributed to weathering and alteration effects, with the presence of chlorite and calcite (Fig. 3m). Hence, it is crucial to assess the alteration effects on the chemical compositions of the analyzed samples. The high-field-strength elements (HFSEs; such as Nb, Ta, Ti, and Hf) and rare Earth elements (REEs) are typically immobile during alteration. This is supported by the consistent elemental variations against the most immobile element Zr, as shown in Fig. S1 in the Supplement. Additionally, Cr (25.4–108 ppm) and Ni (27.4–61.2 ppm) in these samples (except AYBL11D) also demonstrate strong correlations with Zr, suggesting that these elements were essentially immobile during alteration. Based on the Nb/Y vs. Zr/ TiO_2 diagram proposed by Winchester and Floyd (1977), all samples plot in the alkaline series (Fig. 6b). Therefore, we posit that these rocks are best classified as alkaline basalt.

All analyzed samples display consistent chondrite-normalized rare earth element patterns (Fig. 6c), characterized by an enrichment of light rare Earth elements (LREEs) relative to heavy rare Earth elements (HREEs), with $(\text{La}/\text{Yb})_N$ ratios ranging from 6.24 to 7.96. Moreover, their

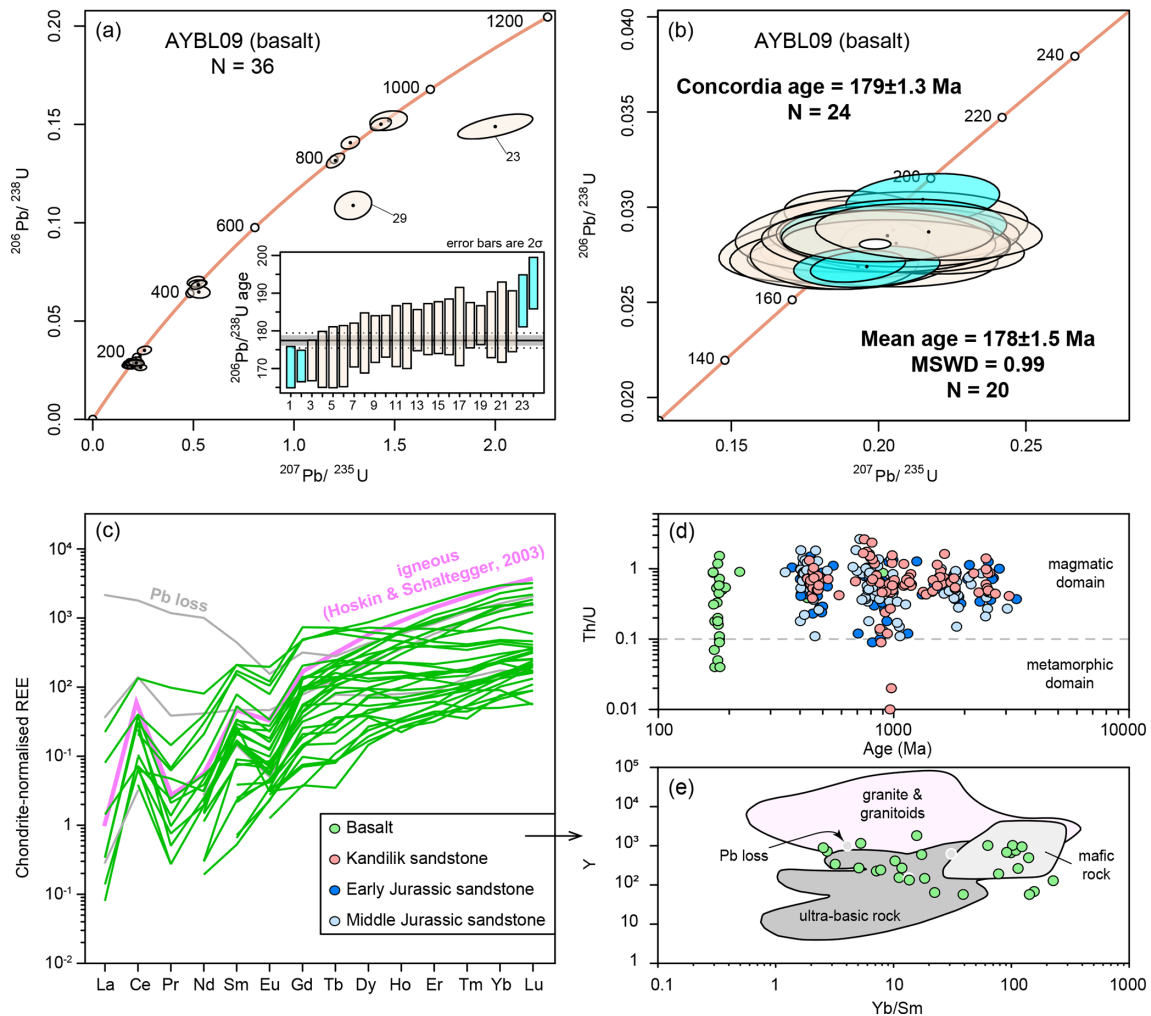


Figure 5. (a) Concordia plot of LA-ICP-MS U–Pb analysis for the zircons of the basalt sample AYBL09. (b) Weighted mean $^{206}\text{Pb}/^{238}\text{U}$ age and concordia age of the youngest zircon groups. (c) Zircon chondrite-normalized REE pattern of the basalt. (d) Th/U ratios of zircons from basalt and sandstone samples. (e) Yb/Sm with Y plotting to distinguish the origins of zircons from the basalt.

REE patterns exhibit slightly negative Eu anomalies ($\delta\text{Eu} = 0.7\text{--}1.0$). The primitive mantle-normalized multi-element diagram illustrates that the analyzed samples are characterized by the enrichment of highly incompatible trace elements relative to low incompatible elements (Fig. 6d). The samples present the significant depletion of Sr and slight enrichment in Zr and Hf. No negative Zr–Hf–Ti anomalies are observed in any of the analyzed basalts.

4.3 Detrital zircon U–Pb ages from Jurassic sandstones

The zircon U–Pb geochronological dataset for the detrital zircons is presented in Table S1. A total of 101 spot analyses were conducted on zircon grains from sample AYBL13. After filtering grains with discordance $> 10\%$, 98 of them met the criteria for inclusion in the kernel density estimate (KDE) visualization (Fig. 7a). The analyzed results reveal that the Th/U ratios of most effective zircons range between 0.12 and

2.61, with only four zircons yielding extremely low values below 0.1 (Fig. 5d). The results suggest that most detrital zircons from sample AYBL13 are of igneous origin (Belousova et al., 2002). The youngest zircon grain from this sandstone yielded an apparent $^{206}\text{Pb}/^{238}\text{U}$ age of 429 ± 5 Ma, whereas the oldest grain has an apparent $^{206}\text{Pb}/^{207}\text{Pb}$ age of 3080 ± 22 Ma. The KDE plot reveals four main age populations with peaks at approximately 446, 820–955, 1553, and 2484 Ma (Fig. 7b).

To analyze provenance, two Jurassic samples from Kyzyltau were analyzed for age comparison. The Early Jurassic sample KZLT1601 underwent 100 spot analyses on randomly selected zircon grains. These measured grains exhibit Th/U ratios ranging from 0.09 to 1.49 (Fig. 5d), consistent with an igneous origin. In total, 89 zircon ages were plotted on or near the concordant curve (Fig. 7c), providing zircon ages ranging from 369 ± 6 to 3314 ± 15 Ma. The detrital age

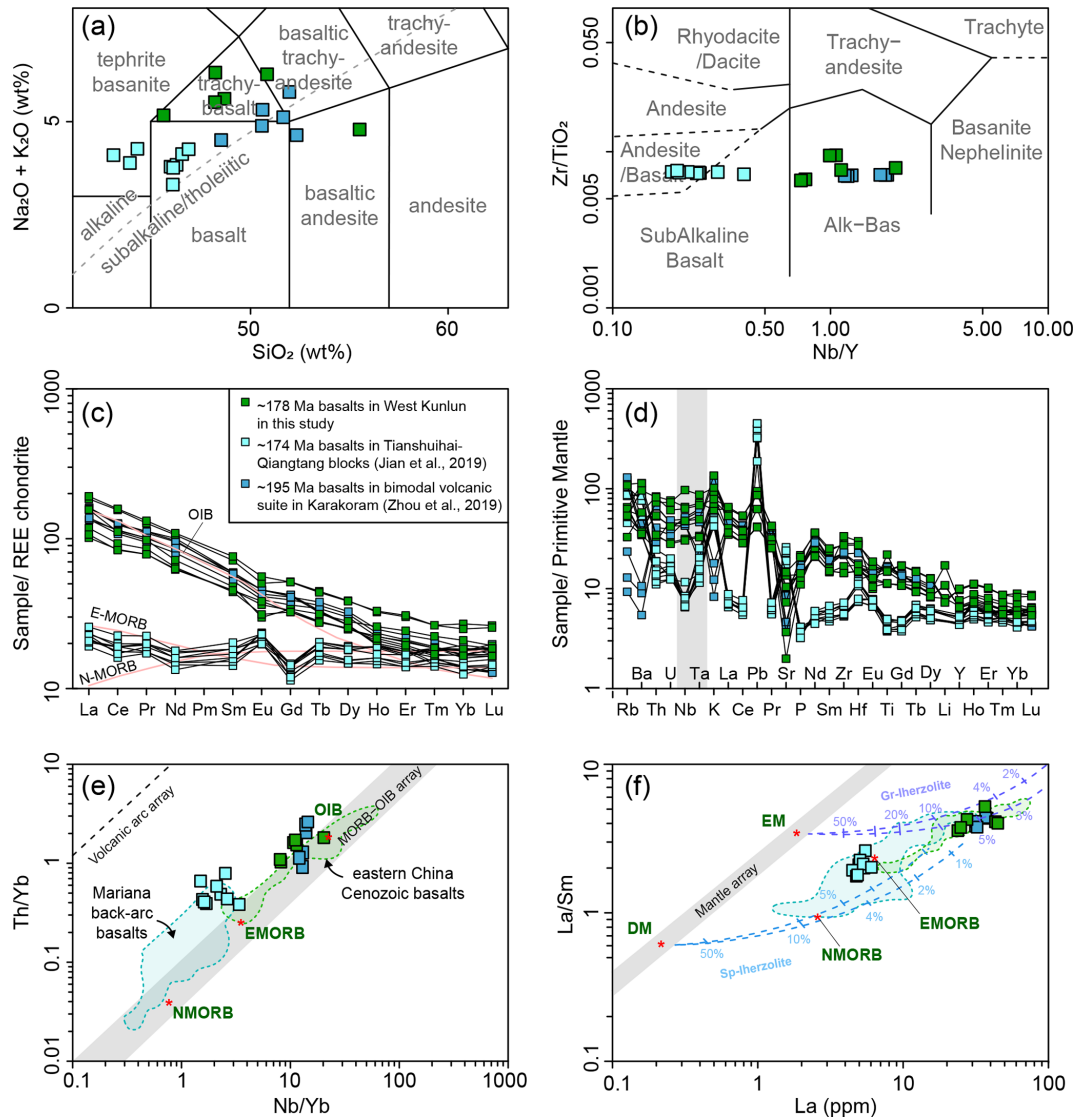


Figure 6. Geochemical classification diagram of Jurassic basalt samples from the Kandilik region in the West Kunlun Mountains (green) and from the Longshan Formation in the Tianshuihai terrane (blue). (a) Total alkali versus silica (Middlemost, 1994) and (b) Zr/TiO_2 vs. Nb/Y diagrams (Winchester and Floyd, 1977). (c) Rare earth element (REE) pattern and (d) trace-element diagrams of Jurassic basalts. (e) Th/Yb vs. Nb/Yb plot (Pearce, 2008) and (f) La/Sm vs. La plot (Aldanmaz et al., 2000). Chondrite-normalized REE and the primitive mantle-normalized values refer to Sun and McDonough (1989). The range of the Mariana back-arc basalts refers to Pearce (2008), and the range of eastern China Cenozoic basalts refers to Guo et al. (2020).

spectrum was obtained using the KDE method and revealed similar peaks at approximately 444, 807, 1823, and 2566 Ma (Fig. 7d).

Similarly, 100 zircon grains from the Middle Jurassic sample KZLT1602 exhibit characteristics indicative of a magmatic origin, with high Th/U ratios ranging between 0.11 and 2.63 (Fig. 5d). A total of 98 concordant results display a consistent age population with the sample KZLT1601, ranging from 345 ± 4 Ma to 3029 ± 15 Ma (Fig. 7e). These age populations on the KDE plot also display four main peaks at approximately 435, 782–988, 1829, and 2480 Ma (Fig. 7f).

4.4 Analysis of Jurassic conglomerate clast lithologies

The field provenance analysis of the Lower Jurassic conglomerate (Shalitashi Formation) reveals significant variations in composition across different sections. In the Kangsu and Wulagen sections, located in the northernmost region of the West Kunlun Range, clasts are composed predominantly of green-colored sandstone (80%–51%) and low-grade metamorphic rocks like schist (0%–46%), with minor occurrences of light-colored siliceous rock (14%–3%) and granitoid (6%–0%). In the northwestern sector of the Pamir, sandstone (22%–46%) and recycled siliceous rock (29%–

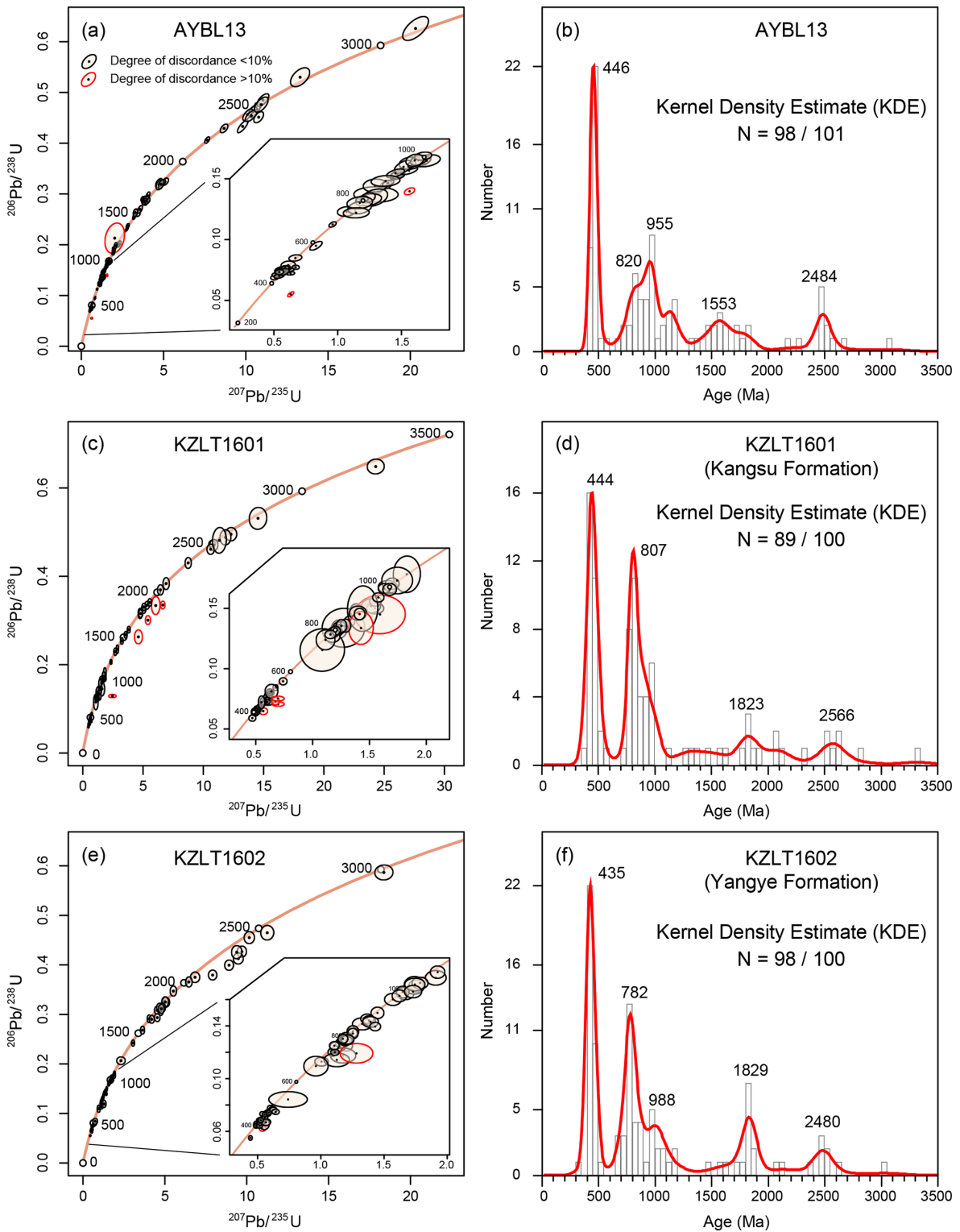


Figure 7. Concordia diagram for the detrital zircons of (a) sample AYBL13 from the Kandilik section, (c) sample KZLT1601 from the Kangsu Formation, and (e) sample KZLT1602 from the Yangye Formation. Diagram of the kernel density estimate of detrital zircon U–Pb ages for (b) AYBL13, (d) KZLT1601, and (f) KZLT1602.

46 %) predominantly constitute major clasts in the Oytag and Gaizi sections, respectively (Fig. 3b and c). Additionally, minor limestone (11 %–2 %) and diverse igneous rocks (38 %–6 %), including granitoid, rhyolite, and basalt occur characteristically in the same stratigraphic horizon. In the Kyzyltau section (Fig. 3d), the clasts of the Jurassic conglomerate are dominated by green-colored sandstone (28 %) and granite (50 %), with subordinate schist (13 %) and siliceous rock (9 %). To the south of Kyzyltau, the Tamu and Qimugen sections present a provenance source dominated by sedimentary rocks. Clasts of limestone (Fig. 3e) and green-colored sandstone account for 85 % and 61 % in the neighboring sections, respectively. The proportion of reddish sandstone in the Qimugen section (33 %) surpasses that in the Tamu section (15 %). The Kusilafu section, located to the north of the Kandilik region, exhibits similar clast lithologies in the conglomerate to the Qimugen section, with a predominance of green-colored sandstone (34 %) and recycled siliceous rock (45 %), along with minor occurrences of reddish sandstone (16 %). Detailed clast lithologies and counting results are presented in the Table S4 in the Supplement.

5 Identification and age constraints for the Lower Jurassic strata

Jurassic strata are largely exposed in the eastern edge of the West Kunlun Mountains and on the southern side along the Talas–Fergana Fault (Fig. 1c). The Jurassic sequences are comprised of coal-bearing siliciclastic rocks with variable thicknesses (Wu et al., 2021). Jurassic volcanic strata have not been previously identified in the West Kunlun Mountains, although a Jurassic tuffaceous succession and Upper Triassic–Lower Jurassic volcanic rocks crop out in the Hindu Kush along the western edge of the Pamir (Brookfield and Hashmat, 2001). Our study has focused on a package of thick clastic rocks intercalated with basaltic lavas that is exposed in the southernmost part of the Jurassic Kyzyltau syncline (Fig. 2). This stratigraphic package was previously considered to be of Mesoproterozoic or Neoproterozoic age due to the lack of fossil records and the presence of low-grade metamorphism (Ma et al., 1991). Lithologically, the clastic member is composed primarily of gray–black mudstone and fine-grained sandstone to siltstone rich in iron and carbonaceous components (Ma et al., 1991). The overlying basalts vary significantly in their thickness and lithological composition and are composed primarily of basaltic volcanic breccia, amygdaloidal, and massive layers (Fig. 3j and k).

Our new results of the zircon U–Pb dating of basalts and sandstones suggest that this rock assemblage is not Precambrian in age, given the widespread appearance of Phanerozoic ages. We suggest that the weighted mean $^{206}\text{Pb}/^{238}\text{U}$ age (~ 178 Ma) from the basalt sample could define the eruptive age of this magmatic episode based on the following lines of evidence. First, these zircons exhibit similar morpho-

logical and CL imaging characteristics (Fig. 4), with the majority of the analyzed grains displaying Th/U ratios indicating their igneous origin (Fig. 5d). Second, the results of our in situ trace-elemental composition of the zircons (Table S2 in the Supplement) indicate that the chondrite-normalized rare earth elements consistently exhibit a left-sloping pattern with positive anomalies in Ce and Sm and negative anomalies in Eu, similar to those of typical igneous zircons (Fig. 5c; Hoskin and Schaltegger, 2003). Third, according to the Y vs. Yb/Sm plot proposed by Belousova et al. (2002), these Jurassic zircons are consistent with the basic or ultrabasic igneous origin (Fig. 5e). Thus, we posit that the crystallization age of the basalt is Toarcian.

To refine the depositional age of the clastic member of the stratigraphy, we have compared the detrital zircon results from the feldspar lithic sandstones with those from the Lower and Middle Jurassic strata in the Kyzyltau region. The sandstone collected from the Kangsu Formation displayed a similar texture and composition to the rocks from the Kandilik region, which are composed of immature and poorly sorted quartz and lithic fragments (Fig. 3n and o). The age patterns of detrital zircons display remarkably similar populations with Early Silurian (~ 440 Ma) and Tonian (~ 800 – 950 Ma) peaks, indicating that sediments of the two investigated areas shared a common provenance. The Lower and Middle Jurassic sedimentary rocks were previously suggested to have been deposited within half-grabens and mostly sourced from the West Kunlun Mountains (Chen et al., 2018). This interpretation aligns with our findings, which indicate that this stratigraphic package comprises thick sequences of laminated mudstone and siltstone, resembling rift-related deposits formed in a relatively proximal and rapidly filling depositional environment.

Accordingly, we propose reassigning this thick package of clastic rocks to the Early–Middle Jurassic age. We demonstrate the structural compatibility of this new stratigraphic scheme. The Lower to Middle Jurassic strata of the Yarkant Formation in the study area consist of a lacustrine sequence rich in coal beds that are structurally bounded to the west by a mylonite zone (Fig. 2b). The redefined stratigraphic sequence is similarly rich in carbonaceous material and is thrust beneath the coal-bearing strata of the Yarkant Formation along an east-verging thrust fault. These units could extend into the NW–SE-striking Jurassic graben, which surprisingly narrows rapidly towards the south without any obvious facies transition (Fig. 1c). The basinward dipping of strata constituted the western limb of the Jurassic syncline, which has a comparable thickness that may extend into the southern area of the Kyzyltau syncline (Fig. 2).

6 Discussion

6.1 Tectonic setting of the Early Jurassic volcanism

The varying SiO₂ contents and low-Mg# values of the basalt samples suggest that they were not derived from primary magmas but likely underwent crustal assimilation and fractional crystallization (AFC) processes. Generally, mantle-derived magmas suffer various degrees of crust contamination en route from magma chambers to the surface (Aitchison and Forrest, 1994). The presence of inherited Paleozoic and Neoproterozoic zircons in these basalts suggests the potential interactions between the ascending magmas and the country rocks (Fig. 5a). However, these basaltic rocks exhibit no negative anomalies of Nb, Ta, and Ti, which are typically depleted in the crust (Fig. 6d). They exhibit low La/Nb ratios (0.53–1.15) and mostly have high Nb/U ratios (37–45), similar to the range of oceanic lavas (La/Nb < 1.2 and Nb/U > 39; Krienitz et al., 2006). Additionally, all basalt samples exhibit low Th/Nb ratios (0.09–0.15), plotting along the MORB–OIB (mid-ocean ridge basalt and ocean island basalt) array of oceanic basalts within the Th/Yb–Nb/Yb diagram (Fig. 6e; Pearce, 2008). These signatures, with little indication of crustal components, suggest that these basalts experienced negligible crustal contamination. They show extremely low Ni and Cr concentrations and slightly negative Eu and Sr anomalies (Fig. 6c and d), likely resulting from fractional crystallization of olivine, clinopyroxene, and plagioclase.

The Early Jurassic episode (178 Ma) of volcanism in the West Kunlun Mountains temporally followed the Cimmerian Orogeny. The eruption of the Early Jurassic basalts was slightly later than the peak metamorphism of high-pressure granulite facies that has been proposed to have occurred between 200 and 185 Ma (Qu et al., 2021). Collisional orogeny commonly transitions from syn-collisional metamorphism to post-collisional unroofing (Dilek and Altunkaynak, 2007, 2010; Zheng et al., 2019). The unroofing phase could generate geochemically varying granitoids and mafic magmatic rocks (Harris et al., 1986; Zhou et al., 2021).

The Jurassic alkali basalts exhibit the enrichment of LREE and HFSEs without obvious crustal signatures (Fig. 6c and d) which is different from the syn-/post-collisional mafic intrusions and granitoids in the West Kunlun Mountains (Liao et al., 2012; Chen et al., 2021). Their compositions display high Th/Yb and Nb/Yb ratios, similar to intraplate OIBs (Fig. 6e). Melt curve modeling of La/Sm vs. La suggests that they were likely generated by the low-degree partial melting (~ 5%) of a garnet lherzolite mantle source (Fig. 6f). This aligns with the Zr–Nb–Y and Zr–Y–Ti triangular plots proposed by Meschede (1986), indicating a within-plate affinity for the studied Jurassic basalts (Fig. 8a and b). They also have high Ti–Zr contents and Ti/V ratios (48–77), consistent with the characteristics of within-plate alkali basalts or OIBs (Fig. 8d and e).

The generation of these magmas can be attributed to one of two mechanisms. The first explanation is that the north Kunlun region experienced a rapid orogenic collapse after Late Triassic collisional orogeny, during which the intra-plate collapse-related volcanism generate the observed basalt flows. We do not find this hypothesis plausible given the implied rapid transition from peak collisional orogeny, including ca. 185 Ma prograde metamorphism (Qu et al., 2021), to collapse and the volcanism recorded at ca. 178 Ma. Many arc–continent or continent–continent collisional orogens, evolving from peak orogenic metamorphism and orogenic collapse to the intraplate stage, collectively persist for tens of millions of years (Dewey, 2005; Weller et al., 2021). Conversely, Early–Middle Jurassic graben and half-graben structures are widely identified by seismic profiles in the southwestern and southeastern Tarim Basin and Qaidam Basin (Cheng et al., 2019; Zhao et al., 2020; Wu et al., 2021; Xia et al., 2024). Jurassic extensional faults have been reported in the eastern Altyn–Tagh range (Chen et al., 2003). A broad plate boundary extensional process may have impacted these orogenic belts and their hinterland regions. Support for this model also includes the expansive extensional rifts developed across the marginal and interior Eurasia during the Early–Middle Jurassic (e.g., Amu Darya, Afghan–Tajik, and Fergana basins; Otto, 1997; Golonka, 2004).

6.2 Jurassic basin formation and implications for sedimentary provenance

The Late Triassic closure of the Paleo-Tethyan Ocean led to collision of the Cimmerian terranes with Eurasia that caused the uplift of the West Kunlun Mountains (Cao et al., 2015). The Triassic stratum is completely absent in the northern Kunlun region and western Tarim Basin (Wu et al., 2021). In the study area, the deformed Upper Paleozoic strata are unconformably overlain by Lower Jurassic conglomerates (Fig. 9).

The Kyzyltau basin preserves the most comprehensive record of the formation and evolution of a post-Cimmerian rift, spanning from its initiation in the Early Jurassic to its inversion in the Late Jurassic (Wu et al., 2021). The basement of this basin varies along-strike, indicating its strong tectonic reworking prior to the Jurassic deposition. It comprises four subdivisions from the north to the southeast: (1) an Early Devonian metasedimentary rock terrane in the Kashgar depression (1–4 in Fig. 9), (2) the Carboniferous island-arc crust and Permian back-arc basin successions in the NW segment of West Kunlun Mountains (5–6 in Fig. 9), (3) an Upper Carboniferous to Middle Permian platform succession in the middle segment (7–11 in Fig. 9), and (4) an Upper Permian clastic formation in the southern part (12–17 in Fig. 9). The massive conglomerate of the Shalitashi Formation indicates rapid infilling of the Jurassic basin during its initial opening stage. An analysis of conglomerate clast lithologies from

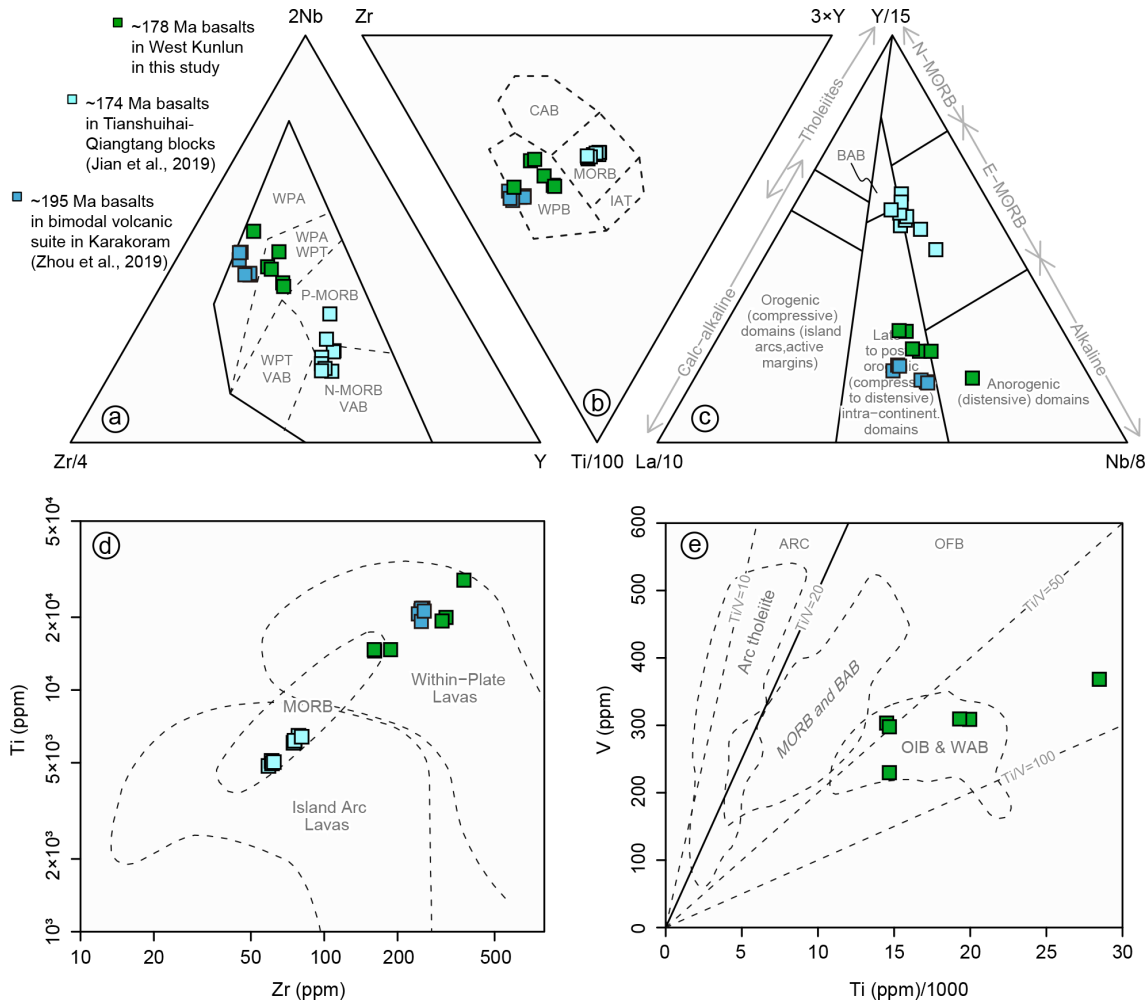


Figure 8. Tectonic discrimination diagrams for Jurassic basalts through (a) Zr/4–2Nb–Y plot, (b) Zr–3Y–Ti/100 plot (Meschede, 1986), (c) La/10–Y/15–Nb/8 plot (Cabanis and Lecolle, 1989), (d) Ti–Zr plot (Pearce, 1982), and (e) V–Ti/1000 plot (Rollinson, 1993). WPB is within-plate basalts; WPA/WAB is within-plate alkali basalts; WPT is within-plate tholeiites; VAB is volcanic-arc basalts; CAB is calc-alkali basalts; IAT is island-arc tholeiites; BAB is back-arc basalts; OIB is ocean island basalts.

different sites suggests significant compositional variations consistent with the presence of local basement rocks (Fig. 9).

The Lower Jurassic strata rapidly transition from alluvial fan deposits into a fluvial sedimentary environment. During the Middle Jurassic, a sequence of stacked coal-bearing sandstones was deposited (Fig. 9). Extensional faulting across the half-grabens further deepened the basin and facilitated the deposition of a turbidite sequence in the Yangye Formation (Wu et al., 2021). Provenance analysis based on detrital zircons suggests that the source region for these sandstones was dominated by Late Ordovician–early Silurian (~ 446–435 Ma) and Neoproterozoic (~ 980–780 Ma) igneous rocks, with minor Neoproterozoic–Paleoproterozoic and Mesoproterozoic ages (Fig. 7). Early Paleozoic (~ 480–440 Ma) granitoids, with a peak intrusive event at ~ 440 Ma (Fig. 1c; Tao et al., 2024), are exposed extensively in the southern Kunlun terrane. However, the southern Kunlun terrane is unlikely

to be the source for these Jurassic depositions because the southern Kunlun region contains extensive Triassic (~ 240–210 Ma) granitoids that intruded into the early Paleozoic rock units (Fig. 1c; Chen et al., 2021). Yet, Triassic detrital zircons are absent in the Lower–Middle Jurassic strata (Fig. 7). Therefore, we instead suggest that the potential source area was most likely the northern Kunlun terrane, which consists mainly of Paleozoic strata and Precambrian metamorphic basements. A provenance study has revealed that the age patterns of detrital zircons from the Ordovician–Devonian strata contain main age peaks at 430–445, 930–800, and 790–760 Ma, with subordinate Neoproterozoic to Mesoproterozoic ages (Yan, 2022). Our results are consistent with this detrital zircon age information from the Lower Paleozoic sedimentary rocks and with the paleocurrent results of previous studies (Wu et al., 2021).

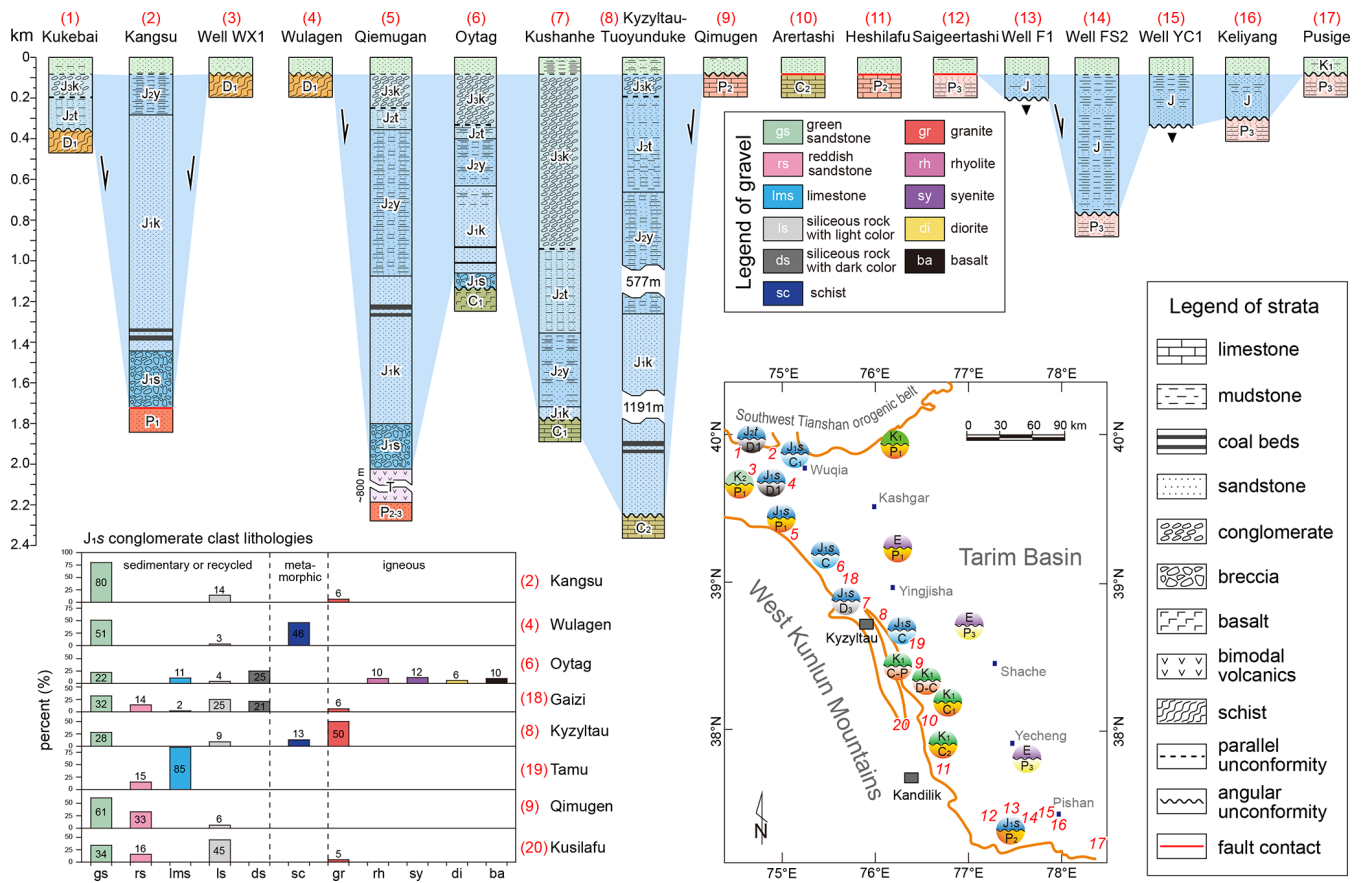


Figure 9. Stratigraphic correlations of the Jurassic basin along the eastern flank of the West Kunlun Mountains (modified from Wu et al., 2021, and Rembe et al., 2022) and the results of gravel analysis of Early Jurassic conglomerate.

A Late Jurassic contractional event affected this region, as evidenced by the intense deformation and metamorphism displayed by various formations and rock units in orogen (Robinson et al., 2007; Groppo et al., 2019), and by the uplift and inversion of the earlier basin (Yang et al., 2017). The Middle Jurassic shallow-marine sequences in southern Qiangtang and SE Pamir were uniformly eroded during this time period (Ma et al., 2023). The Upper Jurassic strata are either entirely absent or locally replaced by conglomerate deposits (Fig. 10). In the Tarim Basin, the Upper Jurassic strata are dominated by brownish–reddish conglomerate. Previous studies have suggested that these red beds may indicate a regional increase in aridity resulting from the uplift of the surrounding mountain belts (Hendrix et al., 1992). The Late Jurassic uplift event has also been supported by numerous thermochronological ages (170–155 Ma) within the West Kunlun Mountains and Pamir (Fig. 1c; Yang et al., 2017). The uplift event also resulted in significant changes in basin and range patterns, and influenced the potential provenance of sediments. The emergence of juvenile detrital zircons in these Upper Jurassic and Lower Cretaceous deposits indicates the exhumation and erosion of a late Paleozoic to Mesozoic arc system (Fig. 10). The Triassic batholiths were thrust

onto the southwestern margin of the Tarim Basin and generated elevated topography, which supplied igneous clastic material to the Cretaceous depocenters in the region.

In summary, the Early Jurassic basin developed on the deformed Paleozoic basement, separated by the Triassic orogenic unconformity. Provenance analysis indicates that the Early to Middle Jurassic sediments were deposited in a half-graben setting and sourced from the proximal basement of the northern Kunlun terrane. This basin was subsequently inverted during the Late Jurassic, driven by the contraction and uplift of the surrounding mountains.

6.3 Switching extensional and contractional tectonics related to the subduction of Neo-Tethys

The Mesozoic era records the transition from the closure of the Paleo-Tethys Ocean to the initiation of subduction within Neo-Tethys (Wan et al., 2019). These processes are influenced by complex plate tectonic conditions, as the evolution of the Paleo- and Neo-Tethys oceans varies significantly in their time–space patterns. The two Tethyan oceans diverge into several branches extending from Iran to Pamir and then eastward into the Tibetan Plateau (Fig. 1a).

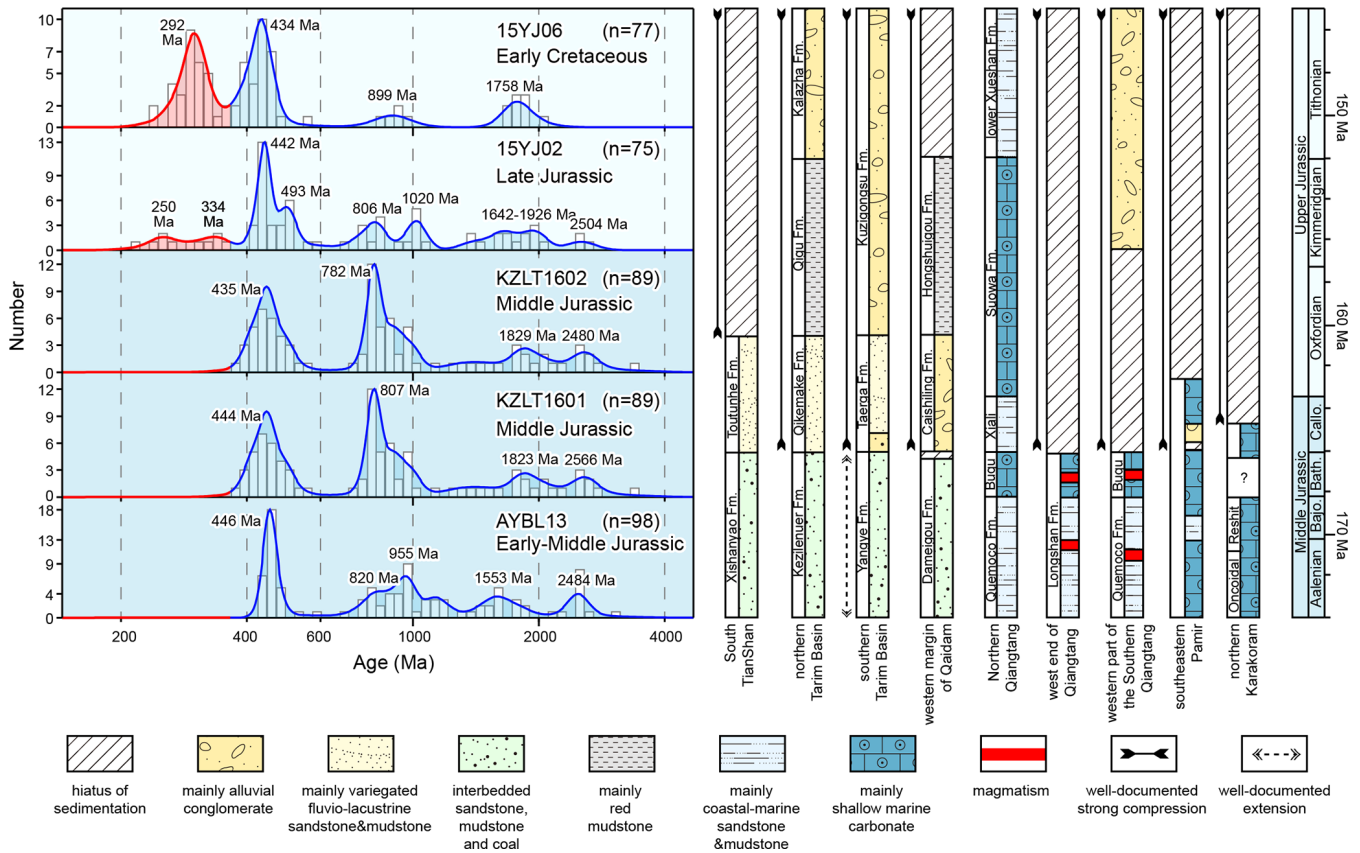


Figure 10. Late Jurassic basin inversion based on the provenance variation through the Early Jurassic to Early Cretaceous and the stratigraphic correlation in the northwestern China. Late Jurassic and Early Cretaceous sandstone samples are according to Zhang et al. (2019b). The sampling locations are shown in Fig. 2a. Stratigraphic correlation is modified from Yang et al. (2017).

Episodic collisions along the southern Asian margin in the Late Triassic and then in the Late Jurassic resulted in major deformation in this region (Jolivet, 2017). Although a flat subduction model has recently been proposed to explain the regional Cretaceous magmatism in the Pamir, the mode of Jurassic tectonic processes remains poorly constrained (Chapman et al., 2018). As discussed above, the history of the Neo-Tethyan subduction events significantly varies spatially. The initiation of subduction along the Tibetan margin occurred during the Middle Triassic, leading to volcanic activities in the southern Lhasa (Wang et al., 2016; Xie and Tang, 2021), whereas the subduction in the Iran sector in the same orogenic belt farther west initiated later in the Early Jurassic (Wan et al., 2023). The extensive Early–Middle arc Jurassic magmatism along both continental margins indicates a synchronous flare-up of continental arcs (Fig. 11a and c). The bimodal volcanism (195–174 Ma) in the Gangdese arc was associated with the subsequent opening of a back-arc basin (174–156 Ma) (Fig. 11c; Kapp and DeCelles, 2019). The magmatic arc of the Sanandaj–Sirjan belt (180–140 Ma) in SW Iran was facilitated by a simultaneous progressive

back-arc rift (Fig. 11a; Hassanzadeh and Wernicke, 2016; Azizi and Stern, 2019).

By comparison, compiled magmatic detrital zircons in the Pamir segment reveal that Early–Middle Jurassic magmatism was almost absent (Fig. 11b; Chapman et al., 2018). Jurassic igneous rocks surrounding the Pamir are also limited (Fig. 7), with only basalts exposed in the northern Kunlun (Kandilik) and Tianshuihai regions (Jian et al., 2019) and bimodal volcanic rock suites found in the east of Karakoram (Zhou et al., 2019). These coeval basaltic lavas (178–174 Ma) exhibit distinct features in their major and trace-element compositions (Fig. 6). Magmas of the basaltic lavas in the northern Kunlun were dominated by within-plate OIBs (Figs. 6 and 8). In contrast, basalts in the Tianshuihai to the south were dominated by back-arc MORBs (Fig. 8a–c), characterized by distinct Nb–Ta depletions (Fig. 6d). The scarcity of zircon-rich felsic magmas in this region evidently differs from the conditions in the western and eastern segments of the Eurasian Tethyan margins, where arc magmatism developed upon continental basement. To date, the exact timing of the onset of subduction-related magmatism in the Pamir Tethyan margin remains unclear. The geochronological dataset for the

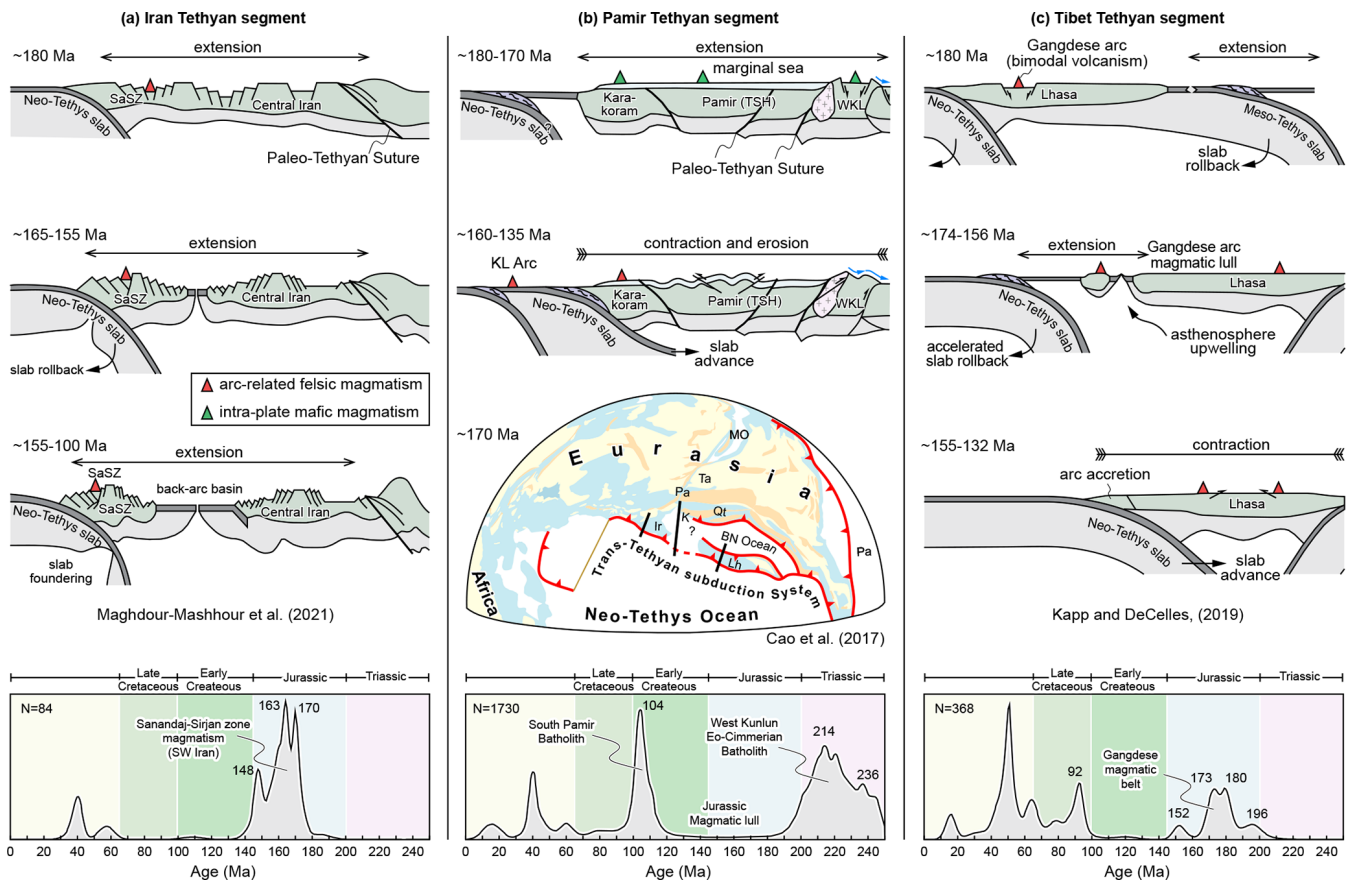


Figure 11. Illustrative cartoons indicating the tectonic variation in the southern Eurasian margin in Jurassic. The subduction of the Neo-Tethys Ocean resulted in persistent rifting along the Iran Tethyan segment, generating massive magmatism during the Early Jurassic to Early Cretaceous. The far-field subduction causing the Early–Middle Jurassic extension along the Pamir Tethyan segment occurred without magmatic flare-up. The changes in subduction style along the Pamir and Tibet Tethyan segments induced the extension–contraction transition. The spatial magmatic datasets are according to Zhang et al. (2018), Chapman et al. (2018), Ma et al. (2017b), and Zhu et al. (2017), and the map of paleogeographic reconstruction is modified from Cao et al. (2017). Tectonic models (a, c) are modified from Maghdour-Mashhour et al. (2021) and Kapp and DeCelles (2019), respectively. SaSZ is the Sanandaj–Sirjan zone; TSH is the Tianshuihai block; WKL is the West Kunlun Mountains; KL Arc is the Kohistan Ladakh Arc; Ir is Iran; K is Karakoram; Pa is Pamir; Ta is Tarim; Qt is Qiangtang; Lh is Lhasa; BN Ocean is Bangong–Nujiang Ocean.

Karakoram arc and the Kohistan Ladakh arc indicates that magmatic activity may have occurred as early as the Late Jurassic (Fig. 11b; Jagoutz et al., 2019; Saktura et al., 2023).

While the spatial continuity of the Tethyan suture zones from Iran into Tibet remains enigmatic, we propose that the regional Early to Middle Jurassic extension across the southern Eurasian continental margin was a consequence of re-creating subduction of the Neo-Tethyan Ocean floor. First, the transition from Cimmerian orogenic build-up (200–185 Ma) to large-scale continental extension (178–174 Ma) suggests the involvement of additional external extensional stresses which are different from the classic cases of continent–continent collision (Weller et al., 2021). Second, the 195 Ma bimodal volcanic rocks in Karakoram and the 174 Ma MORB-like basalts in Tianshuihai have been suggested as associated with the initial opening of a back-arc basin, based

on their geochemical signatures of crustal material metasomatism (Jian et al., 2019; Zhou et al., 2019). The magmatism in Pamir and Karakoram was quite similar to the extensional episodes that occurred in the southern margin of the Lhasa block, caused by accelerated slab rollback (Kapp and DeCelles, 2019). Third, the deposition of shallow-marine carbonates was prevalent in the Pamir and Karakoram during the Middle Jurassic (Fig. 10), indicating an expansive extensional continental platform facing the ocean (Yang et al., 2017). These scenarios are analogous to the active margin of the western Pacific rim, which is characterized by a broad marginal sea with an outboard trench subduction chain (Fig. 1a). Additionally, the Middle Jurassic extension occurred across the broad hinterlands of central Asia, which cannot be easily explained by the collapse of the Paleo-Tethyan orogenic belt (Otto, 1997).

During the Late Jurassic, this marginal extensional basin started to invert, with extensive contractional deformation of the Lower–Middle Jurassic carbonate strata and the development of a major angular unconformity (Fig. 10; Gaetani et al., 1993; Robinson, 2015). Available basement thermochronological data show widespread exhumation across the West Kunlun Mountains (Fig. 1c), as well as the reactivation of the Paleo-Tethyan sutures within the Pamir terranes (Schwab et al., 2004). The exhumation of the Triassic plutons in the southern Kunlun Mountain led to the transport of debris material from the magmatic arc into the Tarim Basin through braided fluvial network systems (Fig. 11b). This broad uplift event has been interpreted as retro-arc deformation and shortening related to the advancing subduction of the Neo-Tethyan Ocean (Robinson, 2015).

The subduction style along the broader strike length of the Tethyan orogen varied from the west to the east in the Late Jurassic–Early Cretaceous. Similar to the West Kunlun Mountains, the Lhasa block to the east experienced basin inversion and contractional deformation starting by ca. 155 Ma and throughout the Early Cretaceous (e.g., Murphy et al., 1997; Ding and Lai, 2003; Kapp and DeCelles, 2019). Geological mapping has documented significant shortening strain (~ 60 %) across Lhasa at this time (Murphy et al., 1997). Although the cause of this event has been debated, the magmatic lull since the earliest Cretaceous and subsequent flare-up in the mid-Cretaceous in both regions imply that they shared a similar geodynamic setting (Fig. 11; Chapman et al., 2018). A major tectonic event involving intense folding and thrusting occurred also around 166 Ma in the South Qiangtang Block, resulting in two phases of southward retreat of the remnant seaway of the Meso-Tethys (Ma et al., 2017a, 2018). A previous study proposed that the development of Jurassic basin inversion in the Tibetan Plateau may be related to the accretion of microcontinents onto the southern Qiangtang margin that is driven by the northward subduction of the Bangong–Nujiang Ocean (Ma et al., 2023). Conversely, the Iranian segment to the west experienced continuous extension at the same time (Hunziker et al., 2015; Lechmann et al., 2018; Maghdour-Mashhour et al., 2021). These along-strike variations likely reflect broad geodynamic changes to, or the initial conditions of, the Tethyan Ocean system that warrant future investigations. For example, variable plate convergence rates related to global tectonic configurations or the oceanic-plate-age variations could result in unique tectonic events along the strike length of the entire Tethyan orogen. Alternatively, the closure of the Bangong–Nujiang Ocean, another branch of the Tethyan system between the Lhasa and Qiangtang blocks, might have also played a significant role in along-strike variations within the Tethyan orogenic belt (Fig. 11; Yang et al., 2017; Kapp and DeCelles, 2019).

7 Conclusion

This study has concentrated on the stratigraphy and provenance of Jurassic strata in the West Kunlun Mountains to better understand the Mesozoic geological evolution of the Eurasian margin within the framework of the Tethyan geodynamics. Our investigations of the Jurassic sedimentary successions, combined with new geochronological and geochemical data from coeval basaltic lava intercalations, led to the following conclusions:

- (1) A newly identified and thick sedimentary package with basaltic lava interlayers in the southern end of the Kyzyltau basin has similarities to the Lower and Middle Jurassic sequences in their clastic compositions and structures. Zircon U–Pb dating results from basaltic lavas suggest an Early Jurassic age (~ 178 Ma) for this stratigraphic member, in contrast to a Precambrian age previously reported. This is a significant change that strongly affects the current tectonic interpretations and models.
- (2) Our new geochemical data from the Early Jurassic basaltic extrusive rocks show that magmas of these basalts had typical OIB affinities and that they lacked crustal contamination. Thus, the related magmatism likely occurred in an intraplate rifting setting and was facilitated by extensional fault systems, which significantly reduced the residence time of the ascending magmas in the crust avoiding contamination.
- (3) Provenance analysis, integrating conglomerate clast lithologies with detrital zircons, indicates a significant source contribution from local basements (northern Kunlun) for the Early to Middle Jurassic rift basins. In comparison, the Late Jurassic contractional event caused an uplift of the surrounding mountains in southern Kunlun and Pamir, significantly influencing the basin tectonostratigraphy and source–sink system.
- (4) The Jurassic switching extensional and contractional tectonics in the West Kunlun Mountains and a wider region across the southern Eurasian margin are related to changes in the subduction style of the Neo-Tethyan Ocean floor, transitioning from retreating in the Early–Middle Jurassic to advancing in the Late Jurassic–Early Cretaceous. Additionally, the Pamir and West Kunlun Mountain regions, as the central junction of the Tethys orogenic belt, share a comparable Mesozoic history of extensional and contractional structures with that of the Tibetan Plateau.

Data availability. The data used in this study are available in the references and in the Supplement, including five tables and one figure.

Supplement. Section S1: Analytical methodology.

Table S1: Zircon U–Pb data of Jurassic basalt and sedimentary rocks.

Table S2: Trace element of zircons.

Table S3: Whole rock geochemical results of Jurassic basalts.

Table S4: Jurassic conglomerate clast lithologies.

Figure S1: Correlations between the trace elements of Jurassic basalts. The supplement related to this article is available online at <https://doi.org/10.5194/se-16-155-2025-supplement>.

Author contributions. HXW: conceptualization, formal analysis, investigation, methodology, visualization, writing (original draft), writing (review and editing), and funding acquisition. HLC: funding acquisition, investigation, and project administration. AVZ and YD: writing (review and editing). DWQ, QYL, and FQZ: investigation and formal analysis. XGC and XBL: investigation.

Competing interests. The contact author has declared that none of the authors has any competing interests.

Disclaimer. Publisher's note: Copernicus Publications remains neutral with regard to jurisdictional claims made in the text, published maps, institutional affiliations, or any other geographical representation in this paper. While Copernicus Publications makes every effort to include appropriate place names, the final responsibility lies with the authors.

Acknowledgement. We gratefully acknowledge the constructive and insightful reviews by two anonymous reviewers and topic editor Yang Chu and the effective editorial handling of Federico Rossetti.

Financial support. This research has been supported by the National Natural Science Foundation of China (grant nos. U22B6002 and 42302231). Hong-Xiang Wu received funding from the Postdoctoral Science Foundation (grant nos. 2023M742979 and 2024T170768).

Review statement. This paper was edited by Yang Chu and reviewed by two anonymous referees.

References

Aitchison, S. J. and Forrest, A. H.: Quantification of Crustal Contamination in Open Magmatic Systems, *J. Petrol.*, 35, 461–488, <https://doi.org/10.1093/petrology/35.2.461>, 1994.

Aldanmaz, E., Pearce, J. A., Thirlwall, M. F., and Mitchell, J. G.: Petrogenetic evolution of late Cenozoic, post-collision volcanism in western Anatolia, Turkey, *J. Volcanol. Geoth. Res.*, 102, 67–95, [https://doi.org/10.1016/S0377-0273\(00\)00182-7](https://doi.org/10.1016/S0377-0273(00)00182-7), 2000.

Andersen, T.: Correction of common lead in U–Pb analyses that do not report ^{204}Pb , *Chem. Geol.*, 192, 59–79, [https://doi.org/10.1016/S0009-2541\(02\)00195-X](https://doi.org/10.1016/S0009-2541(02)00195-X), 2002.

Angiolini, L., Zanchi, A., Zanchetta, S., Nicora, A., and Vezzoli, G.: The Cimmerian geopuzzle: new data from South Pamir, *Terra Nova*, 25, 352–360, <https://doi.org/10.1111/ter.12042>, 2013.

Angiolini, L., Zanchi, A., Zanchetta, S., Nicora, A., Vuolo, I., Berra, F., Henderson, C., Malaspina, N., Rettori, R., Vachard, D., and Vezzoli, G.: From rift to drift in South Pamir (Tajikistan): Permian evolution of a Cimmerian terrane, *J. Asian Earth Sci.*, 102, 146–169, <https://doi.org/10.1016/j.jseae.2014.08.001>, 2015.

Azizi, H. and Stern, R. J.: Jurassic igneous rocks of the central Sanandaj–Sirjan zone (Iran) mark a propagating continental rift, not a magmatic arc, *Terra Nova*, 31, 415–423, <https://doi.org/10.1111/ter.12404>, 2019.

Belousova, E., Griffin, W., O'Reilly, S. Y., and Fisher, N.: Igneous zircon: trace element composition as an indicator of source rock type, *Contrib. Mineral. Petr.*, 143, 602–622, <https://doi.org/10.1007/s00410-002-0364-7>, 2002.

Brookfield, M. E. and Hashmat, A.: The geology and petroleum potential of the North Afghan platform and adjacent areas (northern Afghanistan, with parts of southern Turkmenistan, Uzbekistan and Tajikistan), *Earth-Sci. Rev.*, 55, 41–71, [https://doi.org/10.1016/S0012-8252\(01\)00036-8](https://doi.org/10.1016/S0012-8252(01)00036-8), 2001.

Burtman, V. S. and Molnar, P.: Geological and Geophysical Evidence for Deep Subduction of Continental Crust Beneath the Pamir, in: *Geological and Geophysical Evidence for Deep Subduction of Continental Crust Beneath the Pamir*, Geological Society of America, <https://doi.org/10.1130/SPE281-p1>, 1993.

Cabanis, B. and Lecolle, M.: The La/10-Y/15-Nb/8 diagram: a tool for discriminating volcanic series and evidencing continental crust magmatic mixtures and/or contamination, *CR Acad. Sci. II*, 309, 2023–2029, 1989.

Cao, K., Wang, G.-C., Bernet, M., van der Beek, P., and Zhang, K.-X.: Exhumation history of the West Kunlun Mountains, northwestern Tibet: Evidence for a long-lived, rejuvenated orogen, *Earth Planet. Sc. Lett.*, 432, 391–403, <https://doi.org/10.1016/j.epsl.2015.10.033>, 2015.

Cao, W., Zahirovic, S., Flament, N., Williams, S., Golonka, J., and Müller, R. D.: Improving global paleogeography since the late Paleozoic using paleobiology, *Biogeosciences*, 14, 5425–5439, <https://doi.org/10.5194/bg-14-5425-2017>, 2017.

Chapman, J. B., Scoggin, S. H., Kapp, P., Carrapa, B., Ducea, M. N., Worthington, J., Oimahmadov, I., and Gadoev, M.: Mesozoic to Cenozoic magmatic history of the Pamir, *Earth Planet. Sc. Lett.*, 482, 181–192, <https://doi.org/10.1016/j.epsl.2017.10.041>, 2018.

Chen, S., Chen, H., Zhu, K., and Tao, Y.: Petrogenesis of the Middle–Late Triassic S- and I-type granitoids in the eastern Pamir and implications for the Tanyamas–Jinshajiang Paleo-Tethys Ocean, *Int. J. Earth Sci.*, 110, 1213–1232, <https://doi.org/10.1007/s00531-021-02013-z>, 2021.

Chen, X., Yin, A., Gehrels, G. E., Cowgill, E. S., Grove, M., Harrison, T. M., and Wang, X.-F.: Two phases of Mesozoic north-south extension in the eastern Altyn Tagh range, northern Tibetan Plateau, *Tectonics*, 22, 1053, <https://doi.org/10.1029/2001TC001336>, 2003.

Chen, Y., Wu, H., Zhang, L., Cheng, X., Chen, C., Zhang, Y., Ren, P., Zhang, F., and Chen, H.: Characteristics of the Late Triassic paleo-structure in the mountain front region of western Kunlun

- and its control of Jurassic-Cretaceous deposition, *Chinese Journal of Geology*, 53, 1405–1418, 2018 (in Chinese with English abstract).
- Cheng, F., Jolivet, M., Guo, Z., Lu, H., Zhang, B., Li, X., Zhang, D., Zhang, C., Zhang, H., Wang, L., Wang, Z., and Zhang, Q.: Jurassic–Early Cenozoic Tectonic Inversion in the Qilian Shan and Qaidam Basin, North Tibet: New Insight From Seismic Reflection, Isopach Mapping, and Drill Core Data, *J. Geophys. Res.-Sol. Ea.*, 124, 12077–12098, <https://doi.org/10.1029/2019JB018086>, 2019.
- Corfu, F., Hanchar, J. M., Hoskin, P. W. O., and Kinny, P.: Atlas of Zircon Textures, *Rev. Mineral. Geochem.*, 53, 469–500, <https://doi.org/10.2113/0530469>, 2003.
- Cowgill, E.: Cenozoic right-slip faulting along the eastern margin of the Pamir salient, northwestern China, *GSA Bulletin*, 122, 145–161, <https://doi.org/10.1130/b26520.1>, 2010.
- Dewey, J. F.: Orogeny can be very short, *P. Natl. Acad. Sci. USA*, 102, 15286–15293, <https://doi.org/10.1073/pnas.0505516102>, 2005.
- Dilek, Y. and Altunkaynak, Ş.: Cenozoic Crustal Evolution and Mantle Dynamics of Post-Collisional Magmatism in Western Anatolia, *Int. Geol. Rev.*, 49, 431–453, <https://doi.org/10.2747/0020-6814.49.5.431>, 2007.
- Dilek, Y. and Altunkaynak, Ş.: Geochemistry of Neogene–Quaternary alkaline volcanism in western Anatolia, Turkey, and implications for the Aegean mantle, *Int. Geol. Rev.*, 52, 631–655, <https://doi.org/10.1080/00206810903495020>, 2010.
- Dilek, Y. and Furnes, H.: Tethyan ophiolites and Tethyan seaways, *J. Geol. Soc. London*, 176, 899–912, <https://doi.org/10.1144/jgs2019-129>, 2019.
- Dilek, Y. and Moores, E. M.: Regional tectonics of the eastern Mediterranean ophiolites, in: *Ophiolites. Oceanic Crustal Analogues, Proceedings of the Symposium “Troodos 1987”*, edited by: Malpas, J., Moores, E. M., Panayiotou, A., and Xenophontos, C., The Geological Survey Department, Nicosia, Cyprus, 295–309, 1990.
- Ding, L. and Lai, Q.: New geological evidence of crustal thickening in the Gangdese block prior to the Indo-Asian collision, *Chinese Sci. Bull.*, 48, 1604–1610, <https://doi.org/10.1007/BF03183969>, 2003.
- Dong, Y., He, D., Sun, S., Liu, X., Zhou, X., Zhang, F., Yang, Z., Cheng, B., Zhao, G., and Li, J.: Subduction and accretionary tectonics of the East Kunlun orogen, western segment of the Central China Orogenic System, *Earth-Sci. Rev.*, 186, 231–261, <https://doi.org/10.1016/j.earscirev.2017.12.006>, 2018.
- Faisal, S., Larson, K. P., Cottle, J. M., and Lamming, J.: Building the Hindu Kush: monazite records of terrane accretion, plutonism and the evolution of the Himalaya–Karakoram–Tibet orogen, *Terra Nova*, 26, 395–401, <https://doi.org/10.1111/ter.12112>, 2014.
- Gaetani, M., Jadoul, F., Erba, E., and Garzanti, E.: Jurassic and Cretaceous orogenic events in the North Karakoram: age constraints from sedimentary rocks, *Geological Society, London, Special Publications*, 74, 39–52, <https://doi.org/10.1144/GSL.SP.1993.074.01.04>, 1993.
- Golonka, J.: Plate tectonic evolution of the southern margin of Eurasia in the Mesozoic and Cenozoic, *Tectonophysics*, 381, 235–273, <https://doi.org/10.1016/j.tecto.2002.06.004>, 2004.
- Groppo, C., Rolfo, F., McClelland, W. C., and Coble, M. A.: Pre-Cenozoic evolution of the Aghil Range (western Tibetan Plateau): A missing piece of the Tibet–Pamir–Karakorum geopuzzle, *Gondwana Res.*, 69, 122–143, <https://doi.org/10.1016/j.gr.2018.12.006>, 2019.
- Guo, P., Niu, Y., Sun, P., Gong, H., and Wang, X.: Lithosphere thickness controls continental basalt compositions: An illustration using Cenozoic basalts from eastern China, *Geology*, 48, 128–133, <https://doi.org/10.1130/g46710.1>, 2020.
- Harris, N. B. W., Pearce, J. A., and Tindle, A. G.: Geochemical characteristics of collision-zone magmatism, *Geological Society, London, Special Publications*, 19, 67–81, <https://doi.org/10.1144/GSL.SP.1986.019.01.04>, 1986.
- Hassanzadeh, J. and Wernicke, B. P.: The Neotethyan Sanandaj–Sirjan zone of Iran as an archetype for passive margin–arc transitions, *Tectonics*, 35, 586–621, <https://doi.org/10.1002/2015TC003926>, 2016.
- Hendrix, M. S., Graham, S. A., Carroll, A. R., Sobel, E. R., McKnight, C. L., Schulein, B. J., and Wang, Z.: Sedimentary record and climatic implications of recurrent deformation in the Tian Shan: Evidence from Mesozoic strata of the north Tarim, south Junggar, and Turpan basins, northwest China, *GSA Bulletin*, 104, 53–79, [https://doi.org/10.1130/0016-7606\(1992\)104<0053:Scacio>2.3.Co;2](https://doi.org/10.1130/0016-7606(1992)104<0053:Scacio>2.3.Co;2), 1992.
- Hoskin, P. W. O. and Schaltegger, U.: The Composition of Zircon and Igneous and Metamorphic Petrogenesis, *Rev. Mineral. Geochem.*, 53, 27–62, <https://doi.org/10.2113/0530027>, 2003.
- Hou, Z., Duan, L., Lu, Y., Zheng, Y., Zhu, D., Yang, Z., Wang, B., Pei, Y., Zhao, Z., and McCuaig, T. C.: Lithospheric Architecture of the Lhasa Terrane and Its Control on Ore Deposits in the Himalayan–Tibetan Orogen, *Econ. Geol.*, 110, 1541–1575, <https://doi.org/10.2113/econgeo.110.6.1541>, 2015.
- Hunziker, D., Burg, J.-P., Bouilhol, P., and von Quadt, A.: Jurassic rifting at the Eurasian Tethys margin: Geochemical and geochronological constraints from granitoids of North Makran, southeastern Iran, *Tectonics*, 34, 571–593, <https://doi.org/10.1002/2014TC003768>, 2015.
- Jafari, A., Ao, S., Jamei, S., and Ghasemi, H.: Evolution of the Zagros sector of Neo-Tethys: Tectonic and magmatic events that shaped its rifting, seafloor spreading and subduction history, *Earth-Sci. Rev.*, 241, 104419, <https://doi.org/10.1016/j.earscirev.2023.104419>, 2023.
- Jagoutz, O., Bouilhol, P., Schaltegger, U., and Müntener, O.: The isotopic evolution of the Kohistan Ladakh arc from subduction initiation to continent arc collision, in: *Himalayan Tectonics: A Modern Synthesis*, edited by: Treloar, P. J. and Searle, M. P., The Geological Society of London, <https://doi.org/10.1144/sp483.7>, 2019.
- Jian, K., Gao, F., Du, B., Zhang, Z., Wang, X., and Zhao, D.: Formation age, geochemical characteristics and tectonic setting of the basalts from Longshan Formation in Hweitan area, Karakorum, *J. Mineral. Petrol.*, 39, 42–51, 2019 (in Chinese with English abstract).
- Jolivet, M.: Mesozoic tectonic and topographic evolution of Central Asia and Tibet: a preliminary synthesis, *Geological Society, London, Special Publications*, 427, 19–55, <https://doi.org/10.1144/SP427.2>, 2017.
- Kapp, P. and DeCelles, P. G.: Mesozoic–Cenozoic Geological Evolution of the Himalayan–Tibetan Orogen and

- Working Tectonic Hypotheses, *Am. J. Sci.*, 319, 159–254, <https://doi.org/10.2475/03.2019.01>, 2019.
- Kapp, P., DeCelles, P. G., Gehrels, G. E., Heizler, M., and Ding, L.: Geological records of the Lhasa-Qiangtang and Indo-Asian collisions in the Nima area of central Tibet, *GSA Bulletin*, 119, 917–933, <https://doi.org/10.1130/b26033.1>, 2007.
- Kazmin, V. G.: Collision and rifting in the Tethys Ocean: geodynamic implication, *Tectonophysics*, 196, 371–384, [https://doi.org/10.1016/0040-1951\(91\)90331-L](https://doi.org/10.1016/0040-1951(91)90331-L), 1991.
- Krienitz, M. S., Haase, K. M., Mezger, K., Eckardt, V., and Shaikh-Mashail, M. A.: Magma genesis and crustal contamination of continental intraplate lavas in northwestern Syria, *Contrib. Mineral. Petr.*, 151, 698–716, <https://doi.org/10.1007/s00410-006-0088-1>, 2006.
- Lechmann, A., Burg, J.-P., Ulmer, P., Mohammadi, A., Guillong, M., and Faridi, M.: From Jurassic rifting to Cretaceous subduction in NW Iranian Azerbaijan: geochronological and geochemical signals from granitoids, *Contrib. Mineral. Petr.*, 173, 102, <https://doi.org/10.1007/s00410-018-1532-8>, 2018.
- Leith, W.: A mid-Mesozoic extension across Central Asia?, *Nature*, 313, 567–570, <https://doi.org/10.1038/313567a0>, 1985.
- Li, G., Sandiford, M., Fang, A., Kohn, B., Sandiford, D., Fu, B., Zhang, T., Cao, Y., and Chen, F.: Multi-stage exhumation history of the West Kunlun orogen and the amalgamation of the Tibetan Plateau, *Earth Planet. Sc. Lett.*, 528, 115833, <https://doi.org/10.1016/j.epsl.2019.115833>, 2019.
- Li, L., Najman, Y., Dupont-Nivet, G., Parra, M., Roperch, P., Kaya, M., Meijer, N., O’Sullivan, P., Jepson, G., and Aminov, J.: Mesozoic–Cenozoic multistage tectonic evolution of the Pamir: Detrital fission-track constraints from the Tajik Basin, *Basin Res.*, 35, 530–550, <https://doi.org/10.1111/bre.12721>, 2023.
- Li, S., Zhao, S., Liu, X., Cao, H., Yu, S., Li, X., Somerville, I., Yu, S., and Suo, Y.: Closure of the Proto-Tethys Ocean and Early Paleozoic amalgamation of microcontinental blocks in East Asia, *Earth-Sci. Rev.*, 186, 37–75, <https://doi.org/10.1016/j.earscirev.2017.01.011>, 2018.
- Li, Y., Robinson, A. C., Zucali, M., Gadoev, M., Oimuhhammadzoda, I., Lapen, T. J., and Carrapa, B.: Mesozoic Tectonic Evolution in the Kurgovat-Vanch Complex, NW Pamir, *Tectonics*, 41, e2021TC007180, <https://doi.org/10.1029/2021TC007180>, 2022.
- Liao, S., Jiang, Y., Zhou, Q., Yang, W., Jin, G., and Zhao, P.: Geochemistry and geodynamic implications of the Triassic bimodal magmatism from Western Kunlun Orogen, northwest China, *Int. J. Earth Sci.*, 101, 555–577, <https://doi.org/10.1007/s00531-011-0686-7>, 2012.
- Ma, A., Hu, X., Garzanti, E., Han, Z., and Lai, W.: Sedimentary and tectonic evolution of the southern Qiangtang basin: Implications for the Lhasa-Qiangtang collision timing, *J. Geophys. Res.-Sol. Ea.*, 122, 4790–4813, <https://doi.org/10.1002/2017JB014211>, 2017a.
- Ma, A., Hu, X., Kapp, P., Han, Z., Lai, W., and BouDagher-Fadel, M.: The disappearance of a Late Jurassic remnant sea in the southern Qiangtang Block (Shamuluo Formation, Najiango area): Implications for the tectonic uplift of central Tibet, *Palaeogeogr. Palaeoclimatol.*, 506, 30–47, <https://doi.org/10.1016/j.palaeo.2018.06.005>, 2018.
- Ma, S., Wang, Y., and Fang, X.: Basic characteristics of Proterozoic Eonothem as a table cover on northern slope, *Xinjiang Geology*, 9, 59–71, 1991 (in Chinese with English abstract).
- Ma, X., Xu, Z., Meert, J., and Santosh, M.: Early Jurassic intra-oceanic arc system of the Neotethys Ocean: Constraints from andesites in the Gangdese magmatic belt, south Tibet, *Isl. Arc*, 26, e12202, <https://doi.org/10.1111/iar.12202>, 2017b.
- Ma, A., Hu, X., Garzanti, E., Boudagher-Fadel, M., Xue, W., Han, Z., and Wang, P.: Paleogeographic and tectonic evolution of Mesozoic Qiangtang basins (Tibet), *Tectonophysics*, 862, 229957, <https://doi.org/10.1016/j.tecto.2023.229957>, 2023.
- Maghdour-Mashhour, R., Hayes, B., Pang, K.-N., Bolhar, R., Tabbakh Shabani, A. A., and Elahi-Janatmakan, F.: Episodic subduction initiation triggered Jurassic magmatism in the Sanandaj–Sirjan zone, Iran, *Lithos*, 396–397, 106189, <https://doi.org/10.1016/j.lithos.2021.106189>, 2021.
- Mattern, F. and Schneider, W.: Suturing of the Proto- and Paleotethys oceans in the western Kunlun (Xinjiang, China), *J. Asian Earth Sci.*, 18, 637–650, [https://doi.org/10.1016/S1367-9120\(00\)00011-0](https://doi.org/10.1016/S1367-9120(00)00011-0), 2000.
- Meschede, M.: A method of discriminating between different types of mid-ocean ridge basalts and continental tholeiites with the Nb-Zr-Y diagram, *Chem. Geol.*, 56, 207–218, [https://doi.org/10.1016/0009-2541\(86\)90004-5](https://doi.org/10.1016/0009-2541(86)90004-5), 1986.
- Metcalf, I.: Gondwana dispersion and Asian accretion: Tectonic and palaeogeographic evolution of eastern Tethys, *J. Asian Earth Sci.*, 66, 1–33, <https://doi.org/10.1016/j.jseaes.2012.12.020>, 2013.
- Metcalf, I.: Multiple Tethyan ocean basins and orogenic belts in Asia, *Gondwana Res.*, 100, 87–130, <https://doi.org/10.1016/j.gr.2021.01.012>, 2021.
- Middlemost, E. A. K.: Naming materials in the magma/igneous rock system, *Earth-Sci. Rev.*, 37, 215–224, [https://doi.org/10.1016/0012-8252\(94\)90029-9](https://doi.org/10.1016/0012-8252(94)90029-9), 1994.
- Murphy, M. A., Yin, A., Harrison, T. M., Dürr, S. B., Chen, Z., Ryerson, F. J., Kidd, W. S. F., Wang, X., and Zhou, X.: Did the Indo-Asian collision alone create the Tibetan plateau?, *Geology*, 25, 719–722, [https://doi.org/10.1130/0091-7613\(1997\)025<0719:Dtiaca>2.3.Co;2](https://doi.org/10.1130/0091-7613(1997)025<0719:Dtiaca>2.3.Co;2), 1997.
- Otto, S. C.: Mesozoic–Cenozoic history of deformation and petroleum systems in sedimentary basins of Central Asia; implications of collisions on the Eurasian margin, *Petrol. Geosci.*, 3, 327–341, <https://doi.org/10.1144/petgeo.3.4.327>, 1997.
- Pearce, J. A.: Trace element characteristics of lavas from destructive plate boundaries, in: *Orogenic Andesites and Related Rocks*, edited by: Thorpe, R. S., John Wiley and Sons, Chichester, England, 525–548, ISBN: 9780471280347, 1982.
- Pearce, J. A.: Geochemical fingerprinting of oceanic basalts with applications to ophiolite classification and the search for Archean oceanic crust, *Lithos*, 100, 14–48, <https://doi.org/10.1016/j.lithos.2007.06.016>, 2008.
- Qu, J., Zhang, L., Zhang, J., and Zhang, B.: Petrology and geochronology on high-pressure pelitic granulite from Bulunkuo complex in West Kunlun and its tectonic implication, *Acta Petrol. Sin.*, 37, 563–574, <https://doi.org/10.18654/1000-0569/2021.02.14>, 2021.
- Rembe, J., Sobel, E. R., Kley, J., Terbishaliev, B., Musiol, A., Chen, J., and Zhou, R.: Geochronology, Geochemistry, and Geodynamic Implications of Permo-Triassic Back-Arc Basin Successions in the North Pamir, Central Asia, *Lithosphere*, 2022, 7514691, <https://doi.org/10.2113/2022/7514691>, 2022.

- Robinson, A. C.: Mesozoic tectonics of the Gondwanan terranes of the Pamir plateau, *J. Asian Earth Sci.*, 102, 170–179, <https://doi.org/10.1016/j.jseae.2014.09.012>, 2015.
- Robinson, A. C., Yin, A., Manning, C. E., Harrison, T. M., Zhang, S.-H., and Wang, X.-F.: Cenozoic evolution of the eastern Pamir: Implications for strain-accommodation mechanisms at the western end of the Himalayan-Tibetan orogen, *GSA Bulletin*, 119, 882–896, <https://doi.org/10.1130/b25981.1>, 2007.
- Rollinson, H. R.: *Using Geochemical Data: Evaluation, Presentation, Interpretation, Mineralogical Magazine*, Longman, Edinburgh Gate, London, 352 pp., <https://doi.org/10.4324/9781315845548>, 1993.
- Ruban, D. A., Al-Husseini, M. I., and Iwasaki, Y.: Review of Middle East Paleozoic plate tectonics, *GeoArabia*, 12, 35–56, <https://doi.org/10.2113/geoarabia120335>, 2007.
- Saktura, W. M., Buckman, S., Nutman, A. P., Walsh, J., and Murray, G.: Magmatic records from the Karakoram terrane: U–Pb zircon ages from granites and modern sediments in the Nubra Valley, NW Himalaya, *J. Asian Earth Sci.*, 255, 105771, <https://doi.org/10.1016/j.jseae.2023.105771>, 2023.
- Schwab, M., Ratschbacher, L., Siebel, W., McWilliams, M., Minaev, V., Lutkov, V., Chen, F., Stanek, K., Nelson, B., Frisch, W., and Wooden, J. L.: Assembly of the Pamirs: Age and origin of magmatic belts from the southern Tien Shan to the southern Pamirs and their relation to Tibet, *Tectonics*, 23, TC4002, <https://doi.org/10.1029/2003TC001583>, 2004.
- Şengör, A. M. C.: Mid-Mesozoic closure of Permo–Triassic Tethys and its implications, *Nature*, 279, 590–593, <https://doi.org/10.1038/279590a0>, 1979.
- Şengör, A. M. C.: The Cimmeride Orogenic System and the Tectonics of Eurasia, in: *The Cimmeride Orogenic System and the Tectonics of Eurasia*, Geological Society of America, <https://doi.org/10.1130/SPE195-p1>, 1984.
- Şengör, A. M. C.: Tectonics of the Tethysides: Orogenic Collage Development in a Collisional Setting, *Annu. Rev. Earth Pl. Sc.*, 15, 213–244, <https://doi.org/10.1146/annurev.ea.15.050187.001241>, 1987.
- Şengör, A. M. C., Altner, D., Cin, A., Ustaömer, T., and Hsü, K. J.: Origin and assembly of the Tethyside orogenic collage at the expense of Gondwana Land, *Geological Society, London, Special Publications*, 37, 119–181, <https://doi.org/10.1144/GSL.SP.1988.037.01.09>, 1988.
- Sobel, E. R.: Basin analysis of the Jurassic–Lower Cretaceous southwest Tarim basin, northwest China, *GSA Bulletin*, 111, 709–724, [https://doi.org/10.1130/0016-7606\(1999\)111<0709:Baotjl>2.3.Co;2](https://doi.org/10.1130/0016-7606(1999)111<0709:Baotjl>2.3.Co;2), 1999.
- Sobel, E. R., Chen, J., Schoenbohm, L. M., Thiede, R., Stockli, D. F., Sudo, M., and Strecker, M. R.: Oceanic-style subduction controls late Cenozoic deformation of the Northern Pamir orogen, *Earth Planet. Sc. Lett.*, 363, 204–218, <https://doi.org/10.1016/j.epsl.2012.12.009>, 2013.
- Stampfli, G., Marcoux, J., and Baud, A.: Tethyan margins in space and time, *Palaeogeogr. Palaeoclimatol.*, 87, 373–409, [https://doi.org/10.1016/0031-0182\(91\)90142-E](https://doi.org/10.1016/0031-0182(91)90142-E), 1991.
- Stampfli, G. M.: Tethyan oceans, *Geological Society, London, Special Publications*, 173, 1–23, <https://doi.org/10.1144/GSL.SP.2000.173.01.01>, 2000.
- Stampfli, G. M. and Borel, G. D.: A plate tectonic model for the Paleozoic and Mesozoic constrained by dynamic plate boundaries and restored synthetic oceanic isochrons, *Earth Planet. Sc. Lett.*, 196, 17–33, [https://doi.org/10.1016/S0012-821X\(01\)00588-X](https://doi.org/10.1016/S0012-821X(01)00588-X), 2002.
- Sun, S.-S. and McDonough, W. F.: Chemical and isotopic systematics of oceanic basalts: implications for mantle composition and processes, *Geological Society, London, Special Publications*, 42, 313–345, <https://doi.org/10.1144/GSL.SP.1989.042.01.19>, 1989.
- Tao, Z., Yin, J., Spencer, C. J., Sun, M., Xiao, W., Kerr, A. C., Wang, T., Huangfu, P., Zeng, Y., and Chen, W.: Subduction polarity reversal facilitated by plate coupling during arc-continent collision: Evidence from the Western Kunlun orogenic belt, northwest Tibetan Plateau, *Geology*, 52, 308–313, <https://doi.org/10.1130/g51847.1>, 2024.
- Tapponnier, P., Mattauer, M., Proust, F., and Cassaigneau, C.: Mesozoic ophiolites, sutures, and large-scale tectonic movements in Afghanistan, *Earth Planet. Sc. Lett.*, 52, 355–371, [https://doi.org/10.1016/0012-821X\(81\)90189-8](https://doi.org/10.1016/0012-821X(81)90189-8), 1981.
- Vermeesch, P.: On the visualisation of detrital age distributions, *Chem. Geol.*, 312–313, 190–194, <https://doi.org/10.1016/j.chemgeo.2012.04.021>, 2012.
- Vermeesch, P.: IsoplotR: A free and open toolbox for geochronology, *Geosci. Front.*, 9, 1479–1493, <https://doi.org/10.1016/j.gsf.2018.04.001>, 2018.
- Wan, B., Wu, F., Chen, L., Zhao, L., Liang, X., Xiao, W., and Zhu, R.: Cyclical one-way continental rupture-drift in the Tethyan evolution: Subduction-driven plate tectonics, *Sci. China Earth Sci.*, 62, 2005–2016, <https://doi.org/10.1007/s11430-019-9393-4>, 2019.
- Wan, B., Chu, Y., Chen, L., Zhang, Z., Ao, S., and Talebian, M.: When and Why the Neo-Tethyan Subduction Initiated Along the Eurasian Margin, in: *Compressional Tectonics*, 245–260, <https://doi.org/10.1002/9781119773856.ch9>, 2023.
- Wang, C., Ding, L., Zhang, L.-Y., Kapp, P., Pullen, A., and Yue, Y.-H.: Petrogenesis of Middle–Late Triassic volcanic rocks from the Gangdese belt, southern Lhasa terrane: Implications for early subduction of Neo-Tethyan oceanic lithosphere, *Lithos*, 262, 320–333, <https://doi.org/10.1016/j.lithos.2016.07.021>, 2016.
- Wang, Y., Qian, X., Cawood, P. A., Liu, H., Feng, Q., Zhao, G., Zhang, Y., He, H., and Zhang, P.: Closure of the East Paleotethyan Ocean and amalgamation of the Eastern Cimmerian and Southeast Asia continental fragments, *Earth-Sci. Rev.*, 186, 195–230, <https://doi.org/10.1016/j.earscirev.2017.09.013>, 2018.
- Wei, Y., Zhao, Z., Niu, Y., Zhu, D.-C., Liu, D., Wang, Q., Hou, Z., Mo, X., and Wei, J.: Geochronology and geochemistry of the Early Jurassic Yeba Formation volcanic rocks in southern Tibet: Initiation of back-arc rifting and crustal accretion in the southern Lhasa Terrane, *Lithos*, 278–281, 477–490, <https://doi.org/10.1016/j.lithos.2017.02.013>, 2017.
- Weller, O. M., Mottram, C. M., St-Onge, M. R., Möller, C., Strachan, R., Rivers, T., and Copley, A.: The metamorphic and magmatic record of collisional orogens, *Nature Reviews Earth & Environment*, 2, 781–799, <https://doi.org/10.1038/s43017-021-00218-z>, 2021.
- Winchester, J. A. and Floyd, P. A.: Geochemical discrimination of different magma series and their differentiation products using immobile elements, *Chem. Geol.*, 20, 325–343, [https://doi.org/10.1016/0009-2541\(77\)90057-2](https://doi.org/10.1016/0009-2541(77)90057-2), 1977.
- Wu, C., Yin, A., Zuza, A. V., Zhang, J., Liu, W., and Ding, L.: Pre-Cenozoic geologic history of the central and north-

- ern Tibetan Plateau and the role of Wilson cycles in constructing the Tethyan orogenic system, *Lithosphere*, 8, 254–292, <https://doi.org/10.1130/1494.1>, 2016.
- Wu, F. Y., Wan, B., Zhao, L., Xiao, W. J., and Zhu, R. X.: Tethyan geodynamics, *Acta Petrol. Sin.*, 36, 1627–1674, 2020.
- Wu, H., Cheng, X., Chen, H., Chen, C., Dilek, Y., Shi, J., Zeng, C., Li, C., Zhang, W., Zhang, Y., Lin, X., and Zhang, F.: Tectonic Switch From Triassic Contraction to Jurassic-Cretaceous Extension in the Western Tarim Basin, Northwest China: New Insights Into the Evolution of the Paleo-Tethyan Orogenic Belt, *Front. Earth Sci.*, 9, 636383, <https://doi.org/10.3389/feart.2021.636383>, 2021.
- Xia, Y., Yang, X., Hu, C., Lin, H., and Li, H.: Sedimentary infill of Early-Middle Jurassic in the southeastern Tarim Basin and its constraints on the evolution of the Altyn Tagh Fault in the Northeast Tibet Plateau, *Mar. Petrol. Geol.*, 161, 106657, <https://doi.org/10.1016/j.marpetgeo.2023.106657>, 2024.
- Xiao, W. J., Windley, B. F., Chen, H. L., Zhang, G. C., and Li, J. L.: Carboniferous-Triassic subduction and accretion in the western Kunlun, China: Implications for the collisional and accretionary tectonics of the northern Tibetan Plateau, *Geology*, 30, 295–298, [https://doi.org/10.1130/0091-7613\(2002\)030<0295:Ctsaai>2.0.Co;2](https://doi.org/10.1130/0091-7613(2002)030<0295:Ctsaai>2.0.Co;2), 2002.
- Xiao, W. J., Windley, B. F., Liu, D. Y., Jian, P., Liu, C. Z., Yuan, C., and Sun, M.: Accretionary Tectonics of the Western Kunlun Orogen, China: A Paleozoic–Early Mesozoic, Long-Lived Active Continental Margin with Implications for the Growth of Southern Eurasia, *J. Geol.*, 113, 687–705, <https://doi.org/10.1086/449326>, 2005.
- Xie, F. and Tang, J.: The Late Triassic-Jurassic magmatic belt and its implications for the double subduction of the Neo-Tethys Ocean in the southern Lhasa subterranean, Tibet, *Gondwana Res.*, 97, 1–21, <https://doi.org/10.1016/j.gr.2021.05.007>, 2021.
- Xie, Y. and Dilek, Y.: Detrital zircon U–Pb geochronology and fluvial basin evolution of the Liuqu Conglomerate within the Yarlung Zangbo Suture Zone: A critical geochronometer for the collision tectonics of the Tibetan-Himalayan Orogenic Belt, *Geosystems and Geoenvironment*, 2, 100178, <https://doi.org/10.1016/j.geogeo.2023.100178>, 2023.
- Yan, J.: The early Paleozoic tectono-sedimentary characteristics and the basin-orogen process in south Tarim Basin, School of Earth Sciences, Zhejiang University, Hangzhou, Zhejiang, China, 137 pp., 2022 (in Chinese with English abstract).
- Yang, Y.-T., Guo, Z.-X., and Luo, Y.-J.: Middle-Late Jurassic tectonostratigraphic evolution of Central Asia, implications for the collision of the Karakoram-Lhasa Block with Asia, *Earth-Sci. Rev.*, 166, 83–110, <https://doi.org/10.1016/j.earscirev.2017.01.005>, 2017.
- Zhang, K.-J., Zhang, Y.-X., Tang, X.-C., and Xia, B.: Late Mesozoic tectonic evolution and growth of the Tibetan plateau prior to the Indo-Asian collision, *Earth-Sci. Rev.*, 114, 236–249, <https://doi.org/10.1016/j.earscirev.2012.06.001>, 2012.
- Zhang, Q., Wu, Z., Chen, X., Zhou, Q., and Shen, N.: Proto-Tethys oceanic slab break-off: Insights from early Paleozoic magmatic diversity in the West Kunlun Orogen, NW Tibetan Plateau, *Lithos*, 346–347, 105147, <https://doi.org/10.1016/j.lithos.2019.07.014>, 2019a.
- Zhang, S., Hu, X., and Garzanti, E.: Paleocene initial indentation and early growth of the Pamir as recorded in the western Tarim Basin, *Tectonophysics*, 772, 228207, <https://doi.org/10.1016/j.tecto.2019.228207>, 2019b.
- Zhang, Z., Xiao, W., Ji, W., Majidifard, M. R., Rezaeian, M., Talebian, M., Xiang, D., Chen, L., Wan, B., Ao, S., and Esmaeili, R.: Geochemistry, zircon U–Pb and Hf isotope for granitoids, NW Sanandaj-Sirjan zone, Iran: Implications for Mesozoic-Cenozoic episodic magmatism during Neo-Tethyan lithospheric subduction, *Gondwana Res.*, 62, 227–245, <https://doi.org/10.1016/j.gr.2018.04.002>, 2018.
- Zhao, G., Wang, Y., Huang, B., Dong, Y., Li, S., Zhang, G., and Yu, S.: Geological reconstructions of the East Asian blocks: From the breakup of Rodinia to the assembly of Pangea, *Earth-Sci. Rev.*, 186, 262–286, <https://doi.org/10.1016/j.earscirev.2018.10.003>, 2018.
- Zhao, X., Zhao, J., Zeng, X., Tian, J., Guo, Z., Wang, C., Wang, D., and Hu, C.: Early–Middle Jurassic paleogeography reconstruction in the Western Qaidam Basin: Insights from sedimentology and detrital zircon geochronology, *Mar. Petrol. Geol.*, 118, 104445, <https://doi.org/10.1016/j.marpetgeo.2020.104445>, 2020.
- Zheng, Y., Mao, J., Chen, Y., Sun, W., Ni, P., and Yang, X.: Hydrothermal ore deposits in collisional orogens, *Sci. Bull.*, 64, 205–212, <https://doi.org/10.1016/j.scib.2019.01.007>, 2019.
- Zhou, C.-A., Song, S., Allen, M. B., Wang, C., Su, L., and Wang, M.: Post-collisional mafic magmatism: Insights into orogenic collapse and mantle modification from North Qaidam collisional belt, NW China, *Lithos*, 398–399, 106311, <https://doi.org/10.1016/j.lithos.2021.106311>, 2021.
- Zhou, N., Chen, B., Deng, Z., Sang, M., and Bai, Q.: Discovery and Significance of Early Jurassic Bimodal Volcanic Rocks in Huoshaoyun, Karakoram, *Geoscience*, 33, 990–1002, <https://doi.org/10.19657/j.geoscience.1000-8527.2019.05.06>, 2019 (in Chinese with English abstract).
- Zhu, D.-C., Wang, Q., Cawood, P. A., Zhao, Z.-D., and Mo, X.-X.: Raising the Gangdese Mountains in southern Tibet, *J. Geophys. Res.-Sol. Ea.*, 122, 214–223, <https://doi.org/10.1002/2016JB013508>, 2017.
- Zhu, R., Zhao, P., and Zhao, L.: Tectonic evolution and geodynamics of the Neo-Tethys Ocean, *Sci. China Earth Sci.*, 65, 1–24, <https://doi.org/10.1007/s11430-021-9845-7>, 2022.
- Zuza, A. V. and Yin, A.: Balkatach hypothesis: A new model for the evolution of the Pacific, Tethyan, and Paleo-Asian oceanic domains, *Geosphere*, 13, 1664–1712, <https://doi.org/10.1130/ges01463.1>, 2017.